





## ARTICLE

# PD-1 regulates ILC3-driven intestinal immunity and homeostasis

Nicolas Jacquelot <sup>1,2,3,✉</sup>, Le Xiong <sup>4,5</sup>, Wang H.J. Cao <sup>6</sup>, Qitong Huang <sup>6</sup>, Huiyang Yu <sup>6</sup>, Azin Sayad <sup>7</sup>, Casey J.A. Anttila <sup>4</sup>, Tracey M. Baldwin <sup>4</sup>, Peter F. Hickey <sup>4,5</sup>, Daniela Amann-Zalcenstein <sup>4,5</sup>, Pamela S. Ohashi <sup>7,8</sup>, Stephen L. Nutt <sup>4,5</sup>, Gabrielle T. Belz <sup>4,5,6,†,✉</sup> and Cyril Seillet <sup>4,5,†,✉</sup>

© 2024 The Author(s). Published by Elsevier Inc. on behalf of Society for Mucosal Immunology.

This is an open access article under the CC BY-NC-ND license (<http://creativecommons.org/licenses/by-nc-nd/4.0/>).

Interleukin-(IL) 22 production by intestinal group 3 innate lymphoid cells (ILC3) is critical to maintain gut homeostasis. However, IL-22 needs to be tightly controlled; reduced IL-22 expression is associated with intestinal epithelial barrier defect while its overexpression promotes tumor development. Here, using a single-cell ribonucleic acid sequencing approach, we identified a core set of genes associated with increased IL-22 production by ILC3. Among these genes, programmed cell death 1 (PD-1), extensively studied in the context of cancer and chronic infection, was constitutively expressed on a subset of ILC3. These cells, found in the crypt of the small intestine and colon, displayed superior capacity to produce IL-22. PD-1 expression on ILC3 was dependent on the microbiota and was induced during inflammation in response to IL-23 but, conversely, was reduced in the presence of Notch ligand. PD-1<sup>+</sup> ILC3 exhibited distinct metabolic activity with increased glycolytic, lipid, and polyamine synthesis associated with augmented proliferation compared with their PD-1<sup>-</sup> counterparts. Further, PD-1<sup>+</sup> ILC3 showed increased expression of mitochondrial antioxidant proteins which enable the cells to maintain their levels of reactive oxygen species. Loss of PD-1 signaling in ILC3 led to reduced IL-22 production in a cell-intrinsic manner. During inflammation, PD-1 expression was increased on natural cytotoxicity receptor (NCR)<sup>-</sup> ILC3 while deficiency in PD-1 expression resulted in increased susceptibility to experimental colitis and failure to maintain gut barrier integrity. Collectively, our findings uncover a new function of the PD-1 and highlight the role of PD-1 signaling in the maintenance of gut homeostasis mediated by ILC3 in mice.

*Mucosal Immunology* (2024) 17:371–386; <https://doi.org/10.1016/j.mucimm.2024.03.002>

## INTRODUCTION

The intestinal barrier is a complex interface that both protects the body against opportunistic infections and allows the absorption of nutrients. This layer is composed of epithelial cells which physically delimit the host tissues from the gut luminal contents. In addition, the gut mucosa contains different immune cell types that are strategically located to eliminate potential threats and help to maintain tissue homeostasis.

The cytokine interleukin-22 (IL-22) is a critical regulator of gut immunity and acts directly on epithelial cells of the gut to maintain the integrity of the intestinal barrier. Group 3 innate lymphoid cells (ILC3), composed of natural cytotoxicity receptor (NCR) [natural killer (NK)p46] NCR<sup>+</sup>, NCR<sup>-</sup> and cluster of differentiation (CD)4<sup>+</sup> CC chemokine receptor (CCR)6<sup>+</sup> lymphoid-tissue inducer (LTI)-like cells, are the main source of intestinal IL-22<sup>1</sup>. Constitutive expression of IL-22 has been implicated in multiple aspects of epithelial barrier function including regulation of

epithelial cell growth, production of antibacterial peptides<sup>2</sup>, maintenance of tight junctions<sup>3</sup>, and improved nutrient uptake<sup>4</sup>. IL-22 is protective in the gut as the loss of IL-22 results in dysbiosis, barrier disruption, and increased susceptibility to colitis and infection<sup>5–7</sup>. However, it must be tightly controlled as excessive IL-22 has been linked to the development of cancer<sup>8</sup>. In the small intestine, ILC3-derived IL-22 supports intestinal epithelial regeneration and barrier function<sup>9</sup> which is necessary to protect against inflammatory tissue damage induced by dextran sulfate sodium (DSS)<sup>10</sup>. Several pathways influencing IL-22 expression have been described. During inflammation, IL-23 produced by dendritic cells and intestinal epithelial cells<sup>11,12</sup>, and IL-1β<sup>13</sup>, induces IL-22 production by ILC3, particularly the CD4<sup>+</sup>CCR6<sup>+</sup> subset. In contrast, IL-22 production at steady-state relies mainly on food-derived signals, particularly those that activate the Aryl Hydrocarbon Receptor that is known to support IL-22 production by ILC3<sup>14</sup>. Furthermore, vasoactive intestinal peptide (VIP)

† Both authors equally contributed.

<sup>1</sup>Department of Biochemistry and Molecular Biology, Cumming School of Medicine, University of Calgary, Calgary, Canada. <sup>2</sup>Department of Microbiology, Immunology and Infectious Diseases, Cumming School of Medicine, University of Calgary, Calgary, Canada. <sup>3</sup>Arnie Charbonneau Cancer Research Institute, Calgary, Canada. <sup>4</sup>The Walter and Eliza Hall Institute of Medical Research, 1G Royal Parade, Parkville, Victoria, Australia. <sup>5</sup>Department of Medical Biology, University of Melbourne, Parkville, Australia. <sup>6</sup>Frazer Institute, The University of Queensland, Woolloongabba, Queensland, Australia. <sup>7</sup>Princess Margaret Cancer Centre, University Health Network, Toronto, Canada. <sup>8</sup>Department of Immunology, University of Toronto, Faculty of Medicine, Toronto, Canada. ✉ email: [nicolas.jacquelot@ucalgary.ca](mailto:nicolas.jacquelot@ucalgary.ca) <[g.belz@uq.edu.au](mailto:g.belz@uq.edu.au)> <[seillet@wehi.edu.au](mailto:seillet@wehi.edu.au)>

expression by enteric neurons in response to caloric intake influences ILC3-derived IL-22 secretion<sup>15,16</sup>. Collectively, these studies have revealed important extrinsic signals that influence IL-22 production by intestinal ILC3, however, given the critical role played by this cytokine in intestinal homeostasis, additional intrinsic pathways must further regulate IL-22 expression by these innate immune cells.

To identify novel regulators of IL-22 production in ILC3, we used an unbiased approach consisting of profiling the transcriptional profile of innate lymphoid cells in the small intestine using single-cell ribonucleic acid sequencing (scRNAseq). This identified a cluster of ILC3 expressing IL-22 that was also enriched for programmed cell death 1 (PD-1) expression. PD-1 has been reported to be expressed on the surface of many immune cell types including T cells, dendritic cells, and ILC2<sup>17–20</sup>. PD-1 has been extensively studied in the context of T cell exhaustion in chronic infection and cancer, however, its role during homeostasis and on non-T cell populations remains poorly understood. On ILC2, PD-1 expression was shown to be upregulated following infection and its blockade improved the clearance of pathogens<sup>19</sup>. Increased expression of PD-1 has been reported on tumor-infiltrating ILC2 which was associated with their reduced capacity to proliferate and produce cytokines<sup>21,22</sup>. In this study, we aimed to understand the significance of constitutive PD-1 expression on intestinal ILC3 and how its expression was regulated. The expression of PD-1 was first identified on ILC progenitors although it is dispensable for their development<sup>23,24</sup>. PD-1 has been reported on ILC3 in human decidua and was particularly enriched in LTi-like cells<sup>25</sup>. Recently, PD-1 expression was reported on CCR6<sup>+</sup> ILC3 and involved in the metabolic control of ILC3 upon activation<sup>26</sup>. In absence of PD-1, activated ILC3 upregulated fatty acid oxidation which led to reduced IL-22 expression. However, mice used in this study were in Rag2<sup>-/-</sup> background, which are known to have persistent phosphorylation of Stat-3 in ILC3 and intestinal epithelial cells due to the absence of adaptive immunity<sup>4</sup>, raising questions regarding the role of PD-1 on intestinal ILC3 in immunocompetent wild-type mice. In addition, PD-1 expression acts as a metabolic checkpoint in ILC2 but in contrast to ILC3, PD-1 deficiency resulted in increased glycolysis and reduced fatty acid metabolism in these cells<sup>27</sup>. Altogether, these observations suggest that PD-1 differentially regulates the metabolic activity of ILCs, subsequently impacting their effector functions.

In this study, we investigated how PD-1 expression on mature peripheral ILC3 influenced intestinal immune responses. We demonstrated that NCR<sup>-</sup> ILC3 constitutively expresses PD-1 and that this expression was important for the maintenance of the gut homeostasis. Phenotypic and functional analyses confirmed that PD-1<sup>+</sup> ILC3 were more active and produced increased levels of cytokines such as IL-22 compared with their PD-1<sup>-</sup> counterparts. PD-1 expression was dependent on the microbiota at steady-state and was dynamically upregulated during inflammation and following exposure to IL-23. At steady-state, PD-1<sup>+</sup> ILC3 display increased glycolysis and polyamine synthesis supporting their IL-22 production. Finally, PD-1 deficiency, regardless of the presence of adaptive immune cells, increased the susceptibility of mice to DSS-induced colitis associated with enhanced tissue inflammation and intensified epithelial damage. Collectively, our findings indicate that PD-1 is important to sustain the IL-22 production by NCR<sup>-</sup> ILC3 during both homeostatic and inflammatory conditions in mice.

## RESULTS

### PD-1 is expressed by intestinal NCR<sup>-</sup> ILC3

To identify the pathways that regulate the expression of IL-22 among ILC3, we performed scRNAseq analyses of CD127<sup>+</sup> lymphocytes from the small intestine of C57BL/6 mice (Fig. 1A). We identified seven clusters using unbiased clustering approaches. While clusters two, four, and six comprised different subsets of T cells identified based on high expression of *Cd3e*, *Trac*, and *Trdc*, we identified two ILC3 clusters, clusters zero and three, corresponding to the NCR<sup>+</sup> and NCR<sup>-</sup> subsets, respectively (Figs. 1A and 1B). The reanalysis of the ILC3 subsets revealed three distinct clusters (Fig. 1C). The evaluation of differentially regulated genes among these three clusters showed enrichment of *Il22* expression in cluster two (Fig. 1D, Supplementary Table 1), associated with genes expressed by LTi-like ILC3, including *Vipr2* and *Ccr6*. In this cluster, we also observed enrichment of *Vipr2*, *Ret*, and *Atrnl1* expression, three genes that were previously described to promote IL-22 expression<sup>10,15,28</sup>. Among the top differentially enriched genes was *Pdcd1* (coding for PD-1) (Fig. 1D). To confirm our RNA sequencing data, we examined PD-1 expression on lymphocytes, isolated from the small intestine, colon, and mesenteric lymph nodes (mLN) draining the gut and identified as shown in Supplementary Fig. 1. While NK cells/ILC1 and NCR<sup>+</sup> ILC3 did not express PD-1, we found that ILC2, NCR<sup>-</sup> ILC3 and CD4<sup>+</sup> T cells isolated from the lamina propria of the intestine, colon, and mesenteric lymph nodes constitutively expressed this molecule (Fig. 1E). The frequency of PD-1 expressed on ILC was influenced by the tissue location. PD-1<sup>+</sup> cells were enriched in the colon and small intestine compared to mLN (Fig. 1E). Detailed analysis of the ILC3 subsets revealed that PD-1 expression was found mainly on the CD4<sup>+</sup>(CCR6<sup>+</sup>) subset within NCR<sup>-</sup> ILC3 located in the gut (Fig. 1F).

Next, we analyzed the expression of the programmed death-ligand 1 (PD-L1) on various immune cells residing in the lamina propria and epithelial cells to assess the potential interaction with intestinal PD-1<sup>+</sup> ILC3 (Fig. S2A-C). Our investigation revealed predominant PD-L1 expression on immune cells in both the small intestine and colon. Specifically, myeloid cells, including dendritic cells and macrophages, were the primary sources of PD-L1 expression. Additionally, among lymphocytes, PD-L1 was notably enriched on NK cells/ILC1 and NCR<sup>+</sup> ILC3 (Supplementary Fig. 2). Collectively, our analysis has revealed that *Il22* expressing ILC3 are enriched in *Pdcd1*, and PD-1 expression is restricted to the intestinal CD4<sup>+</sup> LTi-like ILC3 subset.

### PD-1 expression identifies cytokine-producing ILC3

We next sought to further determine the functional differences between the PD-1<sup>+</sup> and PD-1<sup>-</sup> ILC3. ILC3 actively participates in mucosal homeostasis through the constitutive expression of cytokines, in particular IL-22 and granulocyte-macrophage colony-stimulating factor (GM-CSF)<sup>29</sup>. First, we analyzed the constitutive expression of IL-22 in NCR<sup>-</sup> ILC3 isolated from C57BL/6 mice and after stimulation with IL-23. In both the small intestine and colon, PD-1<sup>+</sup> ILC3 expressed higher levels of IL-22 (Figs. 2A and 2B). We also measured the IL-22 expression in Roryt expressing CD4<sup>+</sup> T cells and could not detect differences between the PD-1<sup>+</sup> and PD-1<sup>-</sup> compartments (Figs. 2A and 2B). Roryt<sup>+</sup> cells are poised to produce IL-17, and although the frequencies of IL17<sup>+</sup> cells were relatively small, we were able to detect increased expression in both CD4<sup>+</sup> ILC3 and Roryt<sup>+</sup> CD4<sup>+</sup> T cells in the

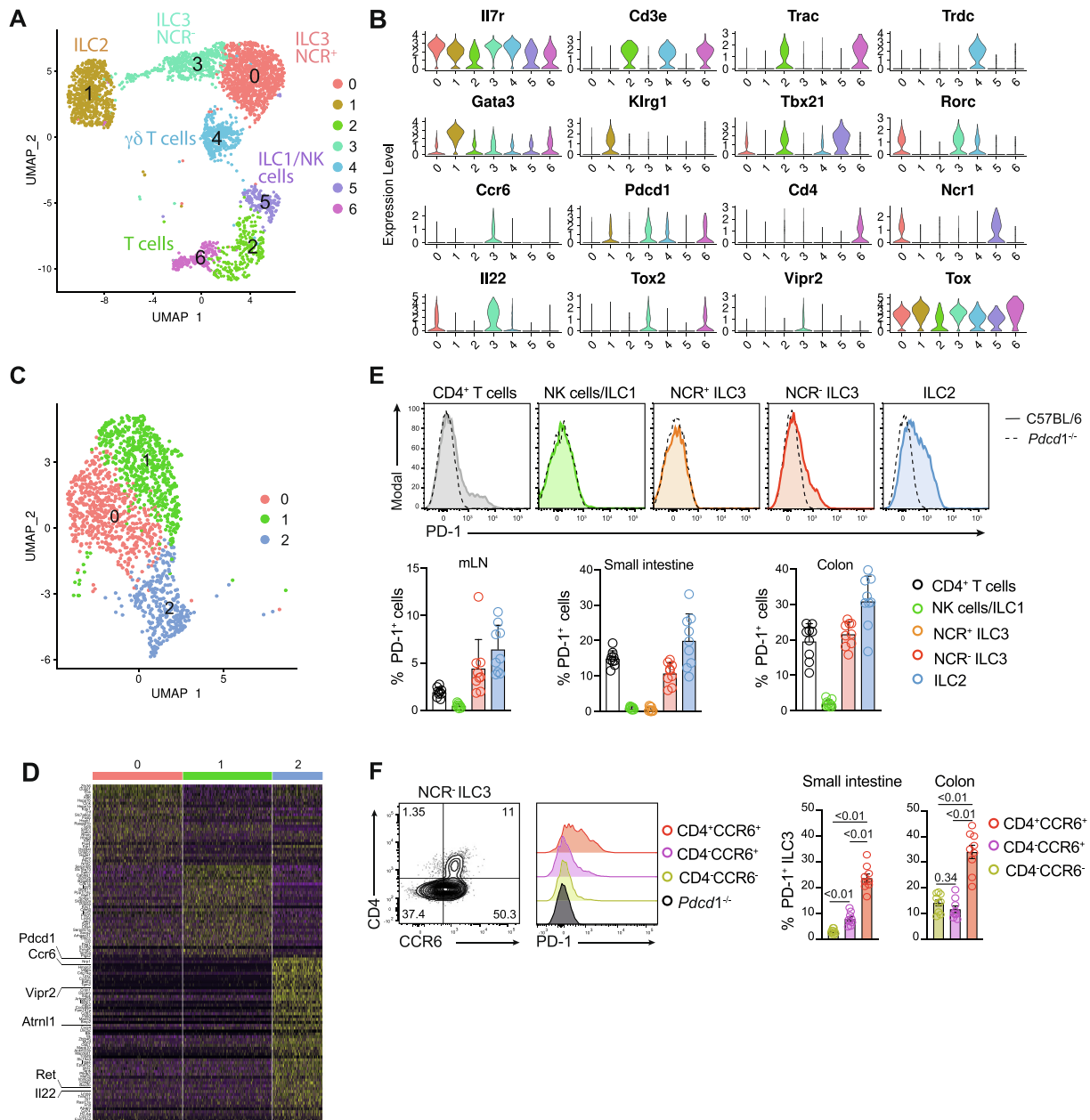


**Fig. 1 Intestinal NCR<sup>+</sup> ILC3 express PD-1.** (A) Unsupervised clustering of Live/Dead<sup>-</sup>CD45<sup>+</sup> Lin<sup>-</sup> (TCR $\beta$ , CD19, B220, CD3, CD11b, CD8 $\alpha$ , F4/80, TER119) CD127<sup>+</sup> immune cells isolated from small intestine of C57BL/6 mice by (UMAP) Uniform Manifold Approximation and Projection. (B) Violin plots showing the expression of signature genes in all clusters. (C) UMAP showing subclusters of ILC3. (D) Heatmap of top differentially expressed genes in ILC3 subsets (Top 60 genes). (E) Analysis of ILC and CD4<sup>+</sup> T cells isolated from the lamina propria of the small intestine, colon, and mesenteric lymph node (mLN) of C57BL/6 and *Pdcd1*<sup>-/-</sup> mice. Histograms of PD-1 expression on immune cell subsets isolated from the small intestine of C57BL/6 (solid line) and *Pdcd1*<sup>-/-</sup> (hatched line) mice. Each dot represents one mouse. Data are pooled from three independent experiments ( $n = 2-3$  mice/experiment). (F) Representative flow cytometry contour plot showing the expression of CD4 and CCR6 among NCR<sup>-</sup> ILC3 (left panel) and histogram (right panel) showing the expression of PD-1 among the indicated subsets isolated from the small intestine of C57BL/6 and *Pdcd1*<sup>-/-</sup> mice. Plots show one representative of 8-9 mice of each genotype from three independent experiments. Bar graphs show the frequency (left panels) and gMFI (right panels) of PD-1 expression on ILC3 subsets. Statistical analyses were performed using paired Student's t tests. The  $p$  values are indicated. CCR = CC chemokine receptor; CD = cluster of differentiation; gMFI = geometric mean fluorescence intensity; ILC3 = intestinal group 3 innate lymphoid cells; mLN = mesenteric lymph node; NCR = natural cytotoxicity receptor; NK, natural killer; PD-1 = programmed cell death 1; TCR = T cell receptor; UMAP = uniform manifold approximation and projection.

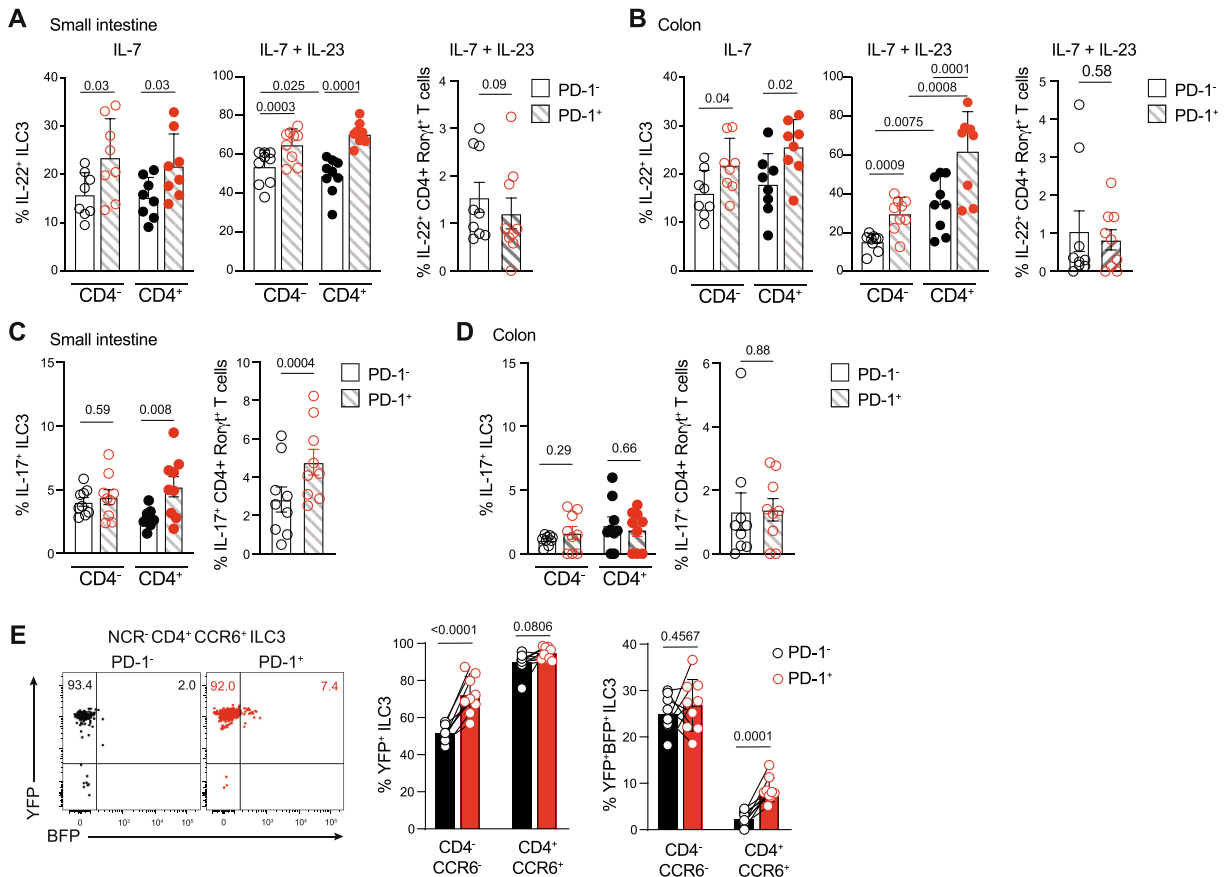


**Fig. 2 PD-1 identifies cytokine producing ILC3.** (A–D) Frequency of IL-22 and IL-17-expressing CD4<sup>-</sup> and CD4<sup>+</sup> NCR<sup>-</sup> ILC3, and CD4<sup>+</sup> Roryt<sup>+</sup> T cells from PD-1 subsets isolated from the small intestine (A, C) and colon (B, D) of C57BL/6 mice. IL-17 and IL-22 expressions were determined following *in vitro* incubation with IL-7 (10 ng/mL; IL-22 only) or IL-7+IL-23 (10 ng/mL each, IL-17 and IL-22) before staining. (E) Representative dot plots (left) and frequency of total GM-CSF production (past and present, YFP) or active GM-CSF expression (YFP<sup>+</sup>BFP<sup>+</sup>) in NCR<sup>-</sup>CD4<sup>+</sup>CCR6<sup>+</sup> ILC3 populations isolated from the small intestine of naive GM-CSF reporter mice (*Csf2*<sup>BFP/YFP</sup>). Live NCR<sup>-</sup> ILC3 were identified as CD45<sup>+</sup> CD3<sup>-</sup> TCRβ<sup>-</sup> CD19<sup>-</sup> CD11b<sup>-</sup> NK1.1<sup>-</sup> KLRG1<sup>-</sup> (lin<sup>-</sup>) NKp46<sup>-</sup>c-kit<sup>+</sup> and then distinguished based on CD4, CCR6 and PD-1 expression; NCR<sup>+</sup> ILC3 as CD45<sup>+</sup> lin<sup>-</sup> NKp46<sup>-</sup> c-kit<sup>low</sup>. (A–E) Each dot represents one mouse. Data show individual mice together with the mean ± SD of data pooled from three independent experiments (*n* = 2–3 mice/experiment). Statistical analyses were performed using analysis of covariance followed by Tukey's multiple comparisons test. The *p* values are indicated. BFP = blue fluorescent protein; CCR = CC chemokine receptor; CD = cluster of differentiation; GM-CSF = granulocyte-macrophage colony-stimulating factor; IL = interleukin; ILC3 = intestinal group 3 innate lymphoid cells; NCR = natural cytotoxicity receptor; NK = natural killer; PD-1 = programmed cell death 1; SD, standard deviation; YFP = yellow fluorescent protein.

small intestine but not the colon (Figs. 2C and 2D). We next determined the expression of GM-CSF using *Csf2*<sup>Cre-BFP</sup> GM-CSF reporter mice which were crossed to *Rosa26*<sup>eYFP</sup>. These dual-reporter mice allowed us to track the active expression of GM-CSF (YFP<sup>+</sup>BFP<sup>+</sup> cells) and cells that exhibited legacy expression of GM-CSF (YFP<sup>+</sup>). Akin to our observations with IL-22, PD-1<sup>+</sup> ILC3 exhibited increased capacity to produce GM-CSF, in particular the CD4<sup>+</sup> ILC3 subset (Fig. 2E) expressing higher levels of PD-1 (Fig. 1F).

To evaluate the role of PD-1 in determining these differences, we investigated how the loss of PD-1 expression impacted the development and function of ILC3 (Fig. 3). No significant changes were observed in the generation of NCR<sup>-</sup> ILC3 irrespective of CD4 surface expression (Figs. 3A–C). While PD-1 expression correlated with increased IL-22 production by NCR<sup>-</sup> ILC3, *Pdcd1*<sup>-/-</sup> NCR<sup>-</sup> ILC3 exhibited reduced IL-22 production, similar to the levels observed in PD-1<sup>-</sup> NCR<sup>-</sup> ILC3 (Fig. 3D). NCR<sup>+</sup> ILC3

from *Pdcd1*<sup>-/-</sup> mice, however, did not show any difference in IL-22 production although these cells increasingly accumulated in the small intestine (Supplementary Figs. 3A and 3C), despite the absence of PD-1 expression on NCR<sup>+</sup> ILC3 (Fig. 1E). The production of IL-22 or IL-17 in CD4<sup>+</sup> Roryt<sup>+</sup> T cells were also not significantly affected in absence of PD-1 (Supplementary Fig. 3B). To determine if the impaired production of IL-22 in *Pdcd1*<sup>-/-</sup> mice was cell-intrinsic, we generated mixed bone marrow (BM) chimeras by reconstituting lethally irradiated (2 × 550 Gy) CD45.1<sup>+/+</sup> mice with an equal ratio of wild-type (F1; CD45.1<sup>+/+</sup>-CD45.2<sup>+/+</sup>) and *Pdcd1*<sup>-/-</sup> (CD45.2<sup>+/+</sup>) BM and allowing recipient mice to reconstitute for 8 weeks (Figs. 3E and 3F and Supplementary Figs. 3D–G). In this setting, NCR<sup>-</sup> ILC3 derived from *Pdcd1*<sup>-/-</sup> BM cells had a similar capacity to produce IL-22 as PD-1<sup>-</sup> NCR<sup>-</sup> ILC3 from C57BL/6 (Figs. 3E and 3F), while the IL-22 production by NCR<sup>+</sup> ILC3 was not affected (Supplementary Fig. 3F). Intriguingly, we also observed the accumulation of

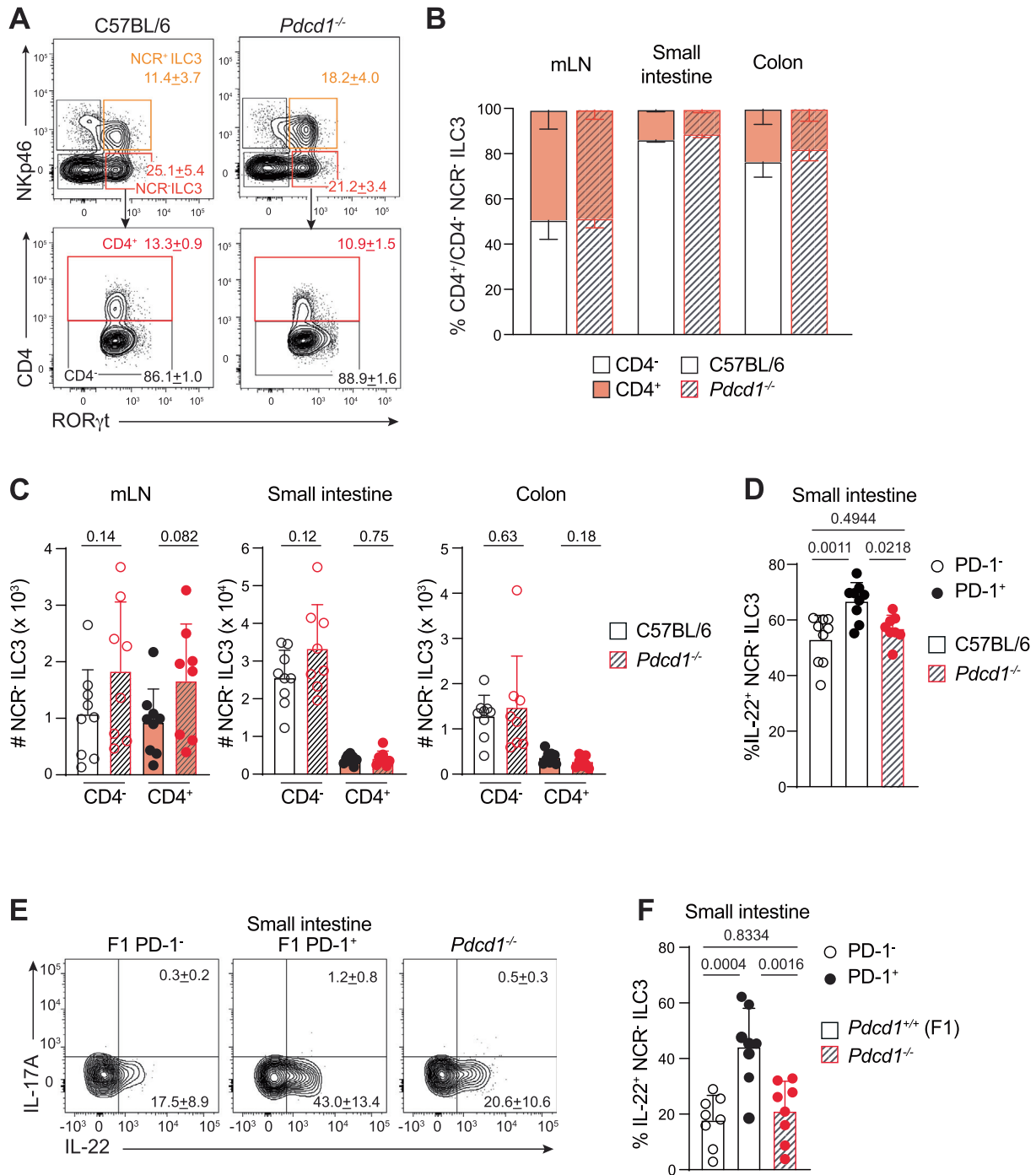
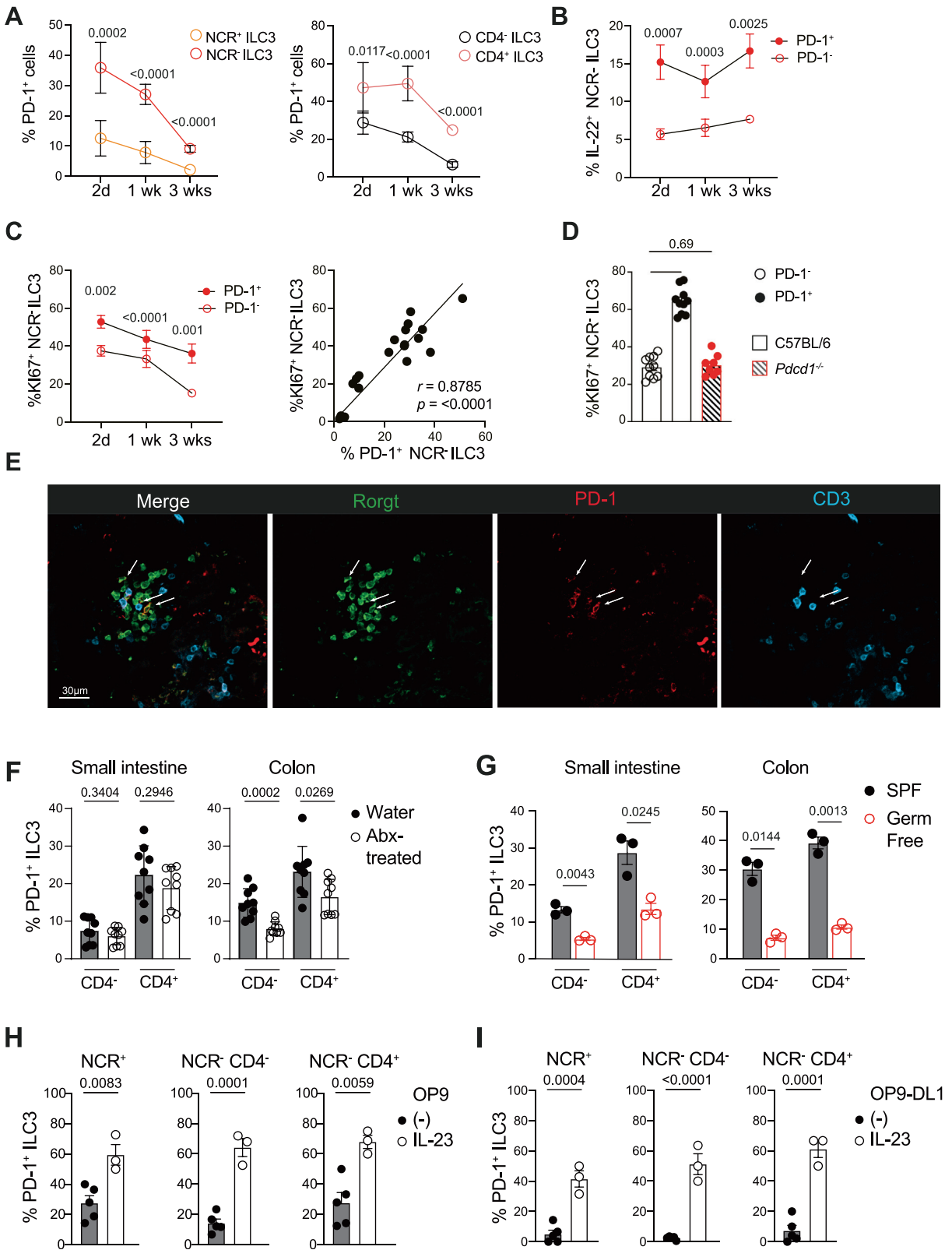


**Fig. 3** Loss of PD-1 negatively impacts IL-22 production by intestinal NCR<sup>-</sup> ILC3. (A–D) Analyses of NCR<sup>-</sup> ILC3 isolated from the lamina propria of the small intestine, colon, and mLN of C57BL/6 and *Pdc1<sup>-/-</sup>* mice. Gating strategy (A), frequencies (B), and total cell number (C) of CD4<sup>+</sup> and CD4<sup>-</sup> NCR<sup>-</sup> ILC3 subsets isolated from the different organs of C57BL/6 and *Pdc1<sup>-/-</sup>* mice. (D) Frequency of IL-22-producing intestinal PD-1<sup>+</sup> and PD-1<sup>-</sup> NCR<sup>-</sup> ILC3 isolated from C57BL/6 and *Pdc1<sup>-/-</sup>* mice. (E and F) Analyses of intestinal NCR<sup>-</sup> ILC3 isolated from mixed BM chimeras after reconstitution with a 1:1 ratio of PD-1 sufficient (C57BL/6 × Ly5.1<sup>+</sup>Ly5.2<sup>+</sup>) and deficient (*Pdc1<sup>-/-</sup>*, Ly5.2<sup>+</sup>) BM (Supplementary Fig. 3D). Representative flow cytometric contour plots of NCR<sup>-</sup> ILC3 (E) and cumulative frequency (F) of IL-22 production from NCR<sup>-</sup> ILC3 from each donor BM. The NCR<sup>-</sup> ILC3 subset originating from PD-1-sufficient BM was split based on PD-1 expression. (A–F) Data show individual mice together with the mean ± SD of data pooled from three independent experiments (n = 8–9 mice with n = 2–3 mice/genotype/experiment). Statistical analyses were performed using unpaired Student's t tests (C) or analysis of covariance followed by Tukey's multiple comparisons test (D and F). The p values are indicated. BM = bone marrow; CD = cluster of differentiation; IL = interleukin; ILC3 = intestinal group 3 innate lymphoid cells; mLN = mesenteric lymph node; NCR = natural cytotoxicity receptor; PD-1 = programmed cell death 1; SD = standard deviation.



NCR<sup>+</sup> ILC3 from the *Pdcd1*<sup>-/-</sup> BM indicating that despite the undetectable expression of PD-1 on NCR<sup>+</sup> ILC3, PD-1 regulates some aspects of the development of these cells (Supplementary Fig. 3G). Altogether, our data show that PD-1 intrinsically increases the capacity of the NCR<sup>-</sup> ILC3 to produce IL-22.

### PD-1<sup>+</sup> ILC3 are enriched in newborn mice

Given that PD-1-expressing cells tend to accumulate in tissue with age<sup>30,31</sup> we asked whether PD-1-expressing ILC might be differentially regulated in naïve newborn and adult mice. Surprisingly, at birth more than 30% of NCR<sup>-</sup> ILC3 expressed PD-1. The frequency of PD-1<sup>+</sup> cells diminished progressively with age to represent 10%–15% of cells at 3 weeks (Fig. 4A) similar to what we observed in adult mice (Figs. 1E and 1F). In addition, a small fraction (10%–15%) of NCR<sup>+</sup> ILC3 isolated from newborn mice also expressed PD-1, potentially explaining the accumulation of NCR<sup>+</sup> ILC3 in *Pdcd1*<sup>-/-</sup> adult mice and chimeras. Over time, the frequency of PD-1<sup>+</sup> ILC3 progressively declined such that intestinal NCR<sup>+</sup> ILC3 from 3-week-old had completely lost PD-1 expression (Fig. 4A). Similarly, we observed a decrease of PD-1 expression in NCR<sup>-</sup> ILC3 but the CD4<sup>+</sup> subset remained the main population that expressed PD-1 compared with CD4<sup>-</sup> ILC3 (Fig. 4A). As in adult mice, PD-1<sup>+</sup> NCR<sup>-</sup> ILC3 had a greater capacity to produce IL-22 at any developmental stage (Fig. 4B). Analyses of cell proliferation indicated by Ki67 expression demonstrated that PD-1<sup>+</sup> NCR<sup>-</sup> ILC3 had also a greater proliferative capacity compared to PD-1<sup>-</sup> counterpart. We observed a strong correlation between the potential of NCR<sup>-</sup> ILC3 to proliferate and the expression of PD-1 (Fig. 4C), suggesting that PD-1 expression by NCR<sup>-</sup> ILC3 also identifies a subset of cells with a higher proliferative capacity. To confirm this observation, we analyzed the proliferation of ILC3 derived from *Pdcd1*<sup>-/-</sup> newborn mice. We found that they exhibited a similar frequency of Ki67<sup>+</sup> cells as PD-1<sup>-</sup> ILC3 highlighting the crucial role of PD-1 to sustain ILC3 proliferation during this early period of life (Fig. 4D).

### PD-1-expressing ILC3 are regulated by the gut microbiota, Notch ligand, and IL-23

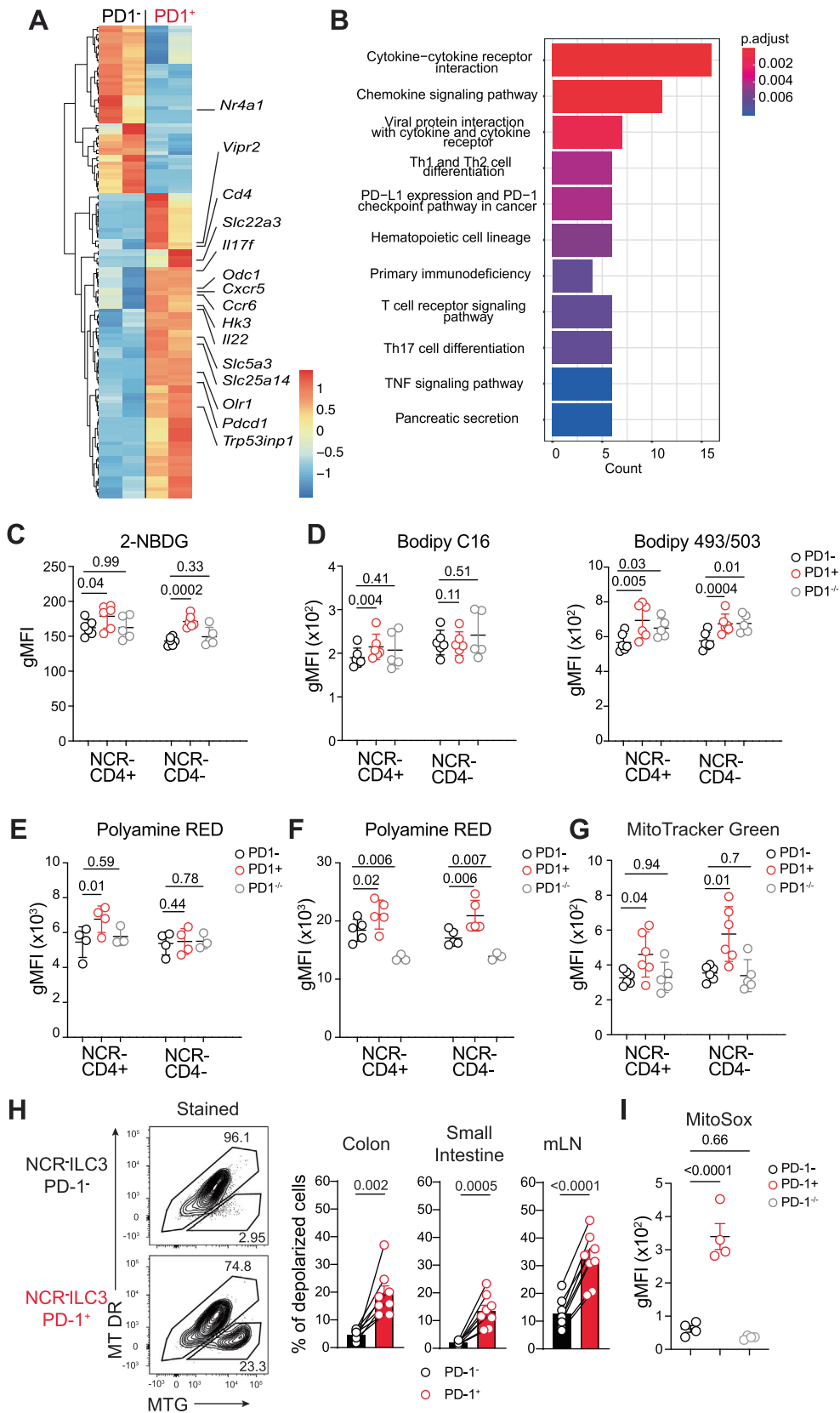
To better appreciate the functional relevance of PD-1<sup>+</sup> ILC3 in the small and large intestines, we analyzed *Roryt*<sup>GFP/+</sup> reporter mice by immunofluorescence to map their tissue distribution.

PD-1<sup>+</sup> ILC3 localized to cryptopatches (Fig. 4E), matching our transcriptional analysis showing that PD-1<sup>+</sup> cells are enriched among LTI-like ILC3<sup>32</sup>.

To investigate the role of the microbiota on the regulation of PD-1 on ILC3, specific pathogen-free C57BL/6 mice were treated with broad-spectrum antibiotics for 3 weeks prior to analysis. In the colon, we observed reduced PD-1 expression on ILC2, ILC3, and CD4<sup>+</sup> T cells in antibiotic-treated mice compared with water controls (Fig. 4F and Supplementary Fig. 4A). However, in the small intestine, only the ILC2 showed a moderate decrease in PD-1 expression while ILC3 and T cells did not show any significant changes. This is in line with our knowledge of the microbial load as there is increased microbiota in the colon than in the small intestine<sup>33</sup>. To further establish the role of the microbiota in PD-1 expression, we analyzed germ-free mice. PD-1 expression by NCR<sup>-</sup> ILC3 was strongly reduced in both the small intestine and colon in the absence of microbiota (Fig. 4G). This reduction was observed in both CD4<sup>-</sup> and CD4<sup>+</sup> NCR<sup>-</sup> ILC3 indicating that both subsets depend on the presence of the microbiota to drive expression of PD-1. In the small intestine, we did not observe significant modification of PD-1 expression on T cells or ILC2 in germ-free mice, however in the colon, ILC2 showed a reduced expression of PD-1 while on T cells, the level of PD-1 was not affected (Supplementary Fig. 4B). This apparent relationship between the presence of the microbiota and the induction of PD-1 expression on ILC3 seemed in contradiction with our previous observation that PD-1 was highly expressed on the first days of birth when the microbial load is low. To test the importance of the microbiota in these early days of life, we compared with specific-pathogen-free and germ-free newborn mice. At day 2 (2d) we did not observe a significant difference in PD-1 expression on the NCR<sup>-</sup> ILC3 subsets, while NCR<sup>+</sup> ILC3 had reduced PD-1 expression in germ-free mice at this stage (Supplementary Fig. 4C). In germ-free pups, PD-1 expressing ILC3 displayed an increased proliferative capacity (Supplementary Fig. 4D) as we previously reported in specific pathogen-free pups (Figs. 4C and 4D). These data suggest that the regulation of PD-1 expression in newborn mice, a window during which ILC3 proliferates, is not driven by the microbiota.

We next aimed to determine which signals could further regulate the PD-1 expression on ILC3. While ILC3 can directly sense microbiota-derived metabolites, they may also become acti-

**Fig. 4 PD-1<sup>+</sup> ILC3 decrease with age and PD-1 expression is dependent on microbiota and IL-23 signaling.** (A) Frequency of PD-1-expressing ILC3 isolated from the small intestine at 2 days, 1 week, 3 week and 8-week-old mice. (B) Frequency of IL-22-producing intestinal PD-1<sup>+</sup> and PD-1<sup>-</sup> NCR<sup>-</sup> ILC3 isolated from C57BL/6 at indicated time point. (C) Frequency of Ki67<sup>+</sup> PD-1<sup>+</sup> and PD-1<sup>-</sup> NCR<sup>-</sup> ILC3 (top panel) and correlation of Ki67<sup>+</sup> NCR<sup>-</sup> ILC3 (bottom panel) relative to PD-1 expression. Correlation was assessed using non-parametric Spearman's test and the coefficient of correlation is indicated. The linear regression curve is overlaid. Data shown from one of two independent experiments. (D) Quantification of Ki67<sup>+</sup> NCR<sup>-</sup> ILC3 in the intestinal tissues of 3-day-old pups from C57BL/6 and *Pdcd1*<sup>-/-</sup> mice. (E) Representative immunofluorescence staining of the intestinal mucosa of *Rorc*( $\gamma$ t)<sup>+/GFP</sup> mice showing, *Roryt* (green), PD-1 (red), and CD3 $\epsilon$  (blue) expression. Arrows indicate PD-1<sup>+</sup> ILC3 in the cryptopatch. (F) Frequency of PD-1-expressing NCR<sup>-</sup> ILC3 isolated from the small intestine and colon of naïve and broad-spectrum antibiotic-treated C57BL/6 mice. Data are pooled from two independent experiments ( $n = 9$  mice/group with 3–6 mice/experiment). (G) Frequency of PD-1-expressing NCR<sup>-</sup> ILC3 isolated from the small intestine and colon of specific pathogen-free and germ-free mice. Data show one of two experiments with similar results ( $n = 3$  mice/group/experiment). H and I, Frequency of PD-1-expressing ILC3 subsets derived from small intestinal PD-1<sup>-</sup> NCR<sup>-</sup> ILC3 from naïve C57BL/6 after 8 days *in vitro* culture with IL-7 in presence (black dots) or without IL-23 (white dots) on OP9 (H) or OP9-DL1 (I) stromal cells. Data show technical replicates (2–3/biological sample) and show one of two independent experiments. (F–I) Each dot shows the results from a single mouse (F–G) or single well (H–I). Data show the mean  $\pm$  SD. Statistical analyses were performed using Student's t tests and  $p$  values are indicated. CD = cluster of differentiation; IL = interleukin; ILC3 = intestinal group 3 innate lymphoid cells; NCR = natural cytotoxicity receptor; PD-1 = programmed cell death 1; SD = standard deviation.





vated through IL-23-derived derived from dendritic cells<sup>34</sup>. To investigate this, we cultured purified intestinal PD-1<sup>-</sup> NCR<sup>-</sup> ILC3 on OP9 stromal cells *in vitro* in the presence or absence of IL-23 for 8 days (Fig. 4H). We found that PD-1<sup>-</sup> NCR<sup>-</sup> ILC3 cultured on OP9 cells upregulated PD-1 across all ILC3 subsets, including *in vitro*-induced NCR<sup>+</sup> ILC3. Furthermore, the addition of IL-23 dramatically induced an increase in the expression of PD-1 (Fig. 4H). Our data are in line with the observations of Wu et al. showing that PD-1 expression on ILC3 is increased following cell activation<sup>26</sup>.

Notch signaling is important for the development of ILC3, and for the emergence of NCR<sup>+</sup> ILC3 from NCR<sup>-</sup> precursors<sup>35,36</sup>. To test the role of Notch signaling on the regulation of PD-1 expression on ILC3, we cultivated purified PD-1<sup>-</sup> NCR<sup>-</sup> intestinal ILC3 with Notch ligand expressing OP9-DL1 stromal cells (Fig. 4I). In this setting, the presence of IL-23 was able to induce PD-1 expression, however, constitutive expression of PD-1 was abolished across all ILC3 subsets (Fig. 4I). Collectively, these results show that the gut microbiota is a key driver of PD-1 expression and that *in vitro* IL-23 promotes PD-1 induction, while Notch signaling inhibits its expression on ILC3. This inhibitory effect of Notch signaling may explain the differential expression of PD-1 on ILC3 subsets as NCR<sup>+</sup> ILC3 require Notch activation for their development from NCR<sup>-</sup> ILC3<sup>35</sup>. Therefore, our data show that PD-1 is dynamically regulated by a combination of signals delivered from the microbial-tissue microenvironment and is expressed on ILC3 specifically localized in the cryptopatches.

### PD-1<sup>+</sup> ILC3 are metabolically distinct from PD-1<sup>-</sup> ILC3

Given that PD-1<sup>+</sup> ILC3 showed the greatest proliferative capacity (Figs. 4C and 4D) and had increased production of cytokines compared with their PD-1<sup>-</sup> counterpart (Fig. 2), we analyzed the transcriptional profile of the NCR<sup>-</sup> PD-1<sup>+</sup> and NCR<sup>-</sup> PD-1<sup>-</sup> ILC3 using bulk RNA sequencing to further identify differentially expressed genes and enriched pathways that could explain the phenotypic heterogeneity and the functional potential of these two subsets (Figs. 5A and 5B). We identified 136 genes differentially expressed between the PD-1<sup>+</sup> and PD-1<sup>-</sup> ILC3 (Supplementary Table 2). Correlating with our scRNAseq data and *ex vivo* phenotyping, we found that genes such as *Ccr6* and *Cd4* were enriched in the PD-1<sup>+</sup> fraction. PD-1<sup>+</sup> ILC3 were also enriched for *Il22* transcript (Fig. 5A). Kyoto Encyclopedia of Genes and

Genomes enrichment pathways further identified genes associated with cytokine interaction and chemokine signaling pathways that are increased in PD-1<sup>+</sup> ILC3 (Fig. 5B) which may correlate with the increased basal activity of these cells. Furthermore, we found several genes associated with metabolic activity including Hexokinase 3 (*Hk3*) involved in glycolytic activity, and ornithine decarboxylase 1 (*Odc1*) which regulates polyamine biosynthesis. Interestingly, increased polyamine and glycolytic activities in ILC3 have been associated with sustained IL-22 production and cell proliferation<sup>37,38</sup>. We also found enriched expression of *Trp53inp1* and *Slc25a14* (also known as mitochondrial uncoupling protein 5, (UCP-5) Mitochondrial uncoupling protein 5) in PD-1<sup>+</sup> ILC3, both molecules supporting cellular antioxidant functions to protect cells against mitochondrial oxidative stress<sup>39,40</sup>. These findings indicate that cytokine-producing ILC3 that express PD-1 display a different metabolic wiring enabling these cells to meet their energy demand.

To further identify differential metabolic activities between PD-1<sup>-</sup> and PD-1<sup>+</sup> ILC3, we next examined the metabolic status of these two populations using the fluorescent metabolic molecules 2-NBDG (2-deoxy-2-[(7-nitro-2,1,3-benzoxadiazol-4-yl)amino]-D-glucose), Bodipy, and PolyamineRED (Figs. 5C–F). PD-1<sup>+</sup> ILC3 showed increased glucose uptake and polyamine accumulation compared to PD-1<sup>-</sup> counterpart or ILC3 isolated from *Pdcd1*<sup>-/-</sup> mice (PD-1<sup>-/-</sup>) (Fig. 5C). Using BodipyFLC<sub>16</sub>, we observed a slight increase in the lipid uptake of the NCR<sup>-</sup> CD4<sup>+</sup> subset but not in CD4<sup>-</sup> fraction. We next used Bodipy 493/503 to monitor the accumulation of lipid droplets in cells. We found an increase in lipid droplets in PD-1<sup>+</sup> ILC3 compared to their PD-1<sup>-</sup> counterparts. However, PD-1<sup>-/-</sup> ILC3 displayed similar accumulation of Bodipy 493/503 to PD-1<sup>+</sup> ILC3 isolated from wild-type animals, suggesting that PD-1<sup>-/-</sup> cells have increased basal lipid biosynthesis (Fig. 5D). We assessed the production of polyamines by staining resting (Fig. 5E) and activated ILC3 (Fig. 5F) with PolyamineRED, an intracellular polyamine detection reagent. NCR<sup>-</sup>CD4<sup>+</sup> PD-1<sup>+</sup> ILC3 showed increased basal PolyamineRED staining compared to PD-1<sup>-</sup> or PD-1<sup>-/-</sup> cells (Fig. 5E), while under stimulation both CD4<sup>-</sup> and CD4<sup>+</sup> showed greater accumulation of polyamines in PD-1 expressing ILC3 (Fig. 5F).

We then investigated mitochondrial function using the fluorescent probes MitoTracker Green and MitoTracker Deep Red to

**Fig. 5 PD-1<sup>+</sup> ILC3 are transcriptionally and metabolically different from PD-1<sup>-</sup> ILC3** (A, B) (RNA) ribonucleic acid sequencing analysis of NCR<sup>-</sup> PD-1<sup>+</sup> and NCR<sup>-</sup> PD-1<sup>-</sup> ILC3. Genes were considered as differentially regulated with a log<sub>2</sub> fold change 1x and adjusted *p* < 0.1. (A) Heatmap show the differentially regulated genes among the PD-1<sup>+</sup> and PD-1<sup>-</sup> subsets. (B) Pathway-enrichment analysis with the KEGG database on differentially expressed genes. (C–F) NCR<sup>-</sup> ILC3 isolated from C57BL/6 and *Pdcd1*<sup>-/-</sup> mice were stained with 2-NBDG and Bodipy<sup>TM</sup>FLC<sub>16</sub>, Bodipy<sub>493/503</sub> fluorescent analogues or PolyamineRED as indicated. ILC3 were directly stained after isolation (C–E) or purified and cultivated overnight in presence of IL-7 (F). (G) NCR<sup>-</sup> ILC3 isolated from C57BL/6 and *Pdcd1*<sup>-/-</sup> mice were stained with MitoTracker Green. The gMFI is shown. Each dot represents one mouse and data show the mean ± SD. Data show one representative experiment of two similar experiments (*n* = 3–6 mice/genotype/experimental group). (H) Gating strategy, representative contour plots and quantification of the proportion of depolarized NCR<sup>-</sup> ILC3 PD-1<sup>+</sup> or PD-1<sup>-</sup> stained for MitoTracker Green and MitoTracker DeepRed, indicative of the mitochondrial mass and membrane potential of the cells, respectively. Data show the pool of 2 independent experiments with 3–5 mice/experiment. (I) NCR<sup>-</sup> ILC3 isolated from C57BL/6 and *Pdcd1*<sup>-/-</sup> mice were stained with MitoSOX Red. The gMFI is shown. Statistical analyses were performed using paired Student's *t* tests and *p* values are indicated. CD = cluster of differentiation; gMFI = geometric mean fluorescence intensity; IL, interleukin; ILC3 = intestinal group 3 innate lymphoid cells; KEGG = Kyoto Encyclopedia of Genes and Genomes; mLN = mesenteric lymph node; 2-NBDG = 2-deoxy-2-[(7-nitro-2,1,3-benzoxadiazol-4-yl)amino]-D-glucose; NCR = natural cytotoxicity receptor; PD-1 = programmed cell death 1; RNA = ribonucleic acid; SD, standard deviation.

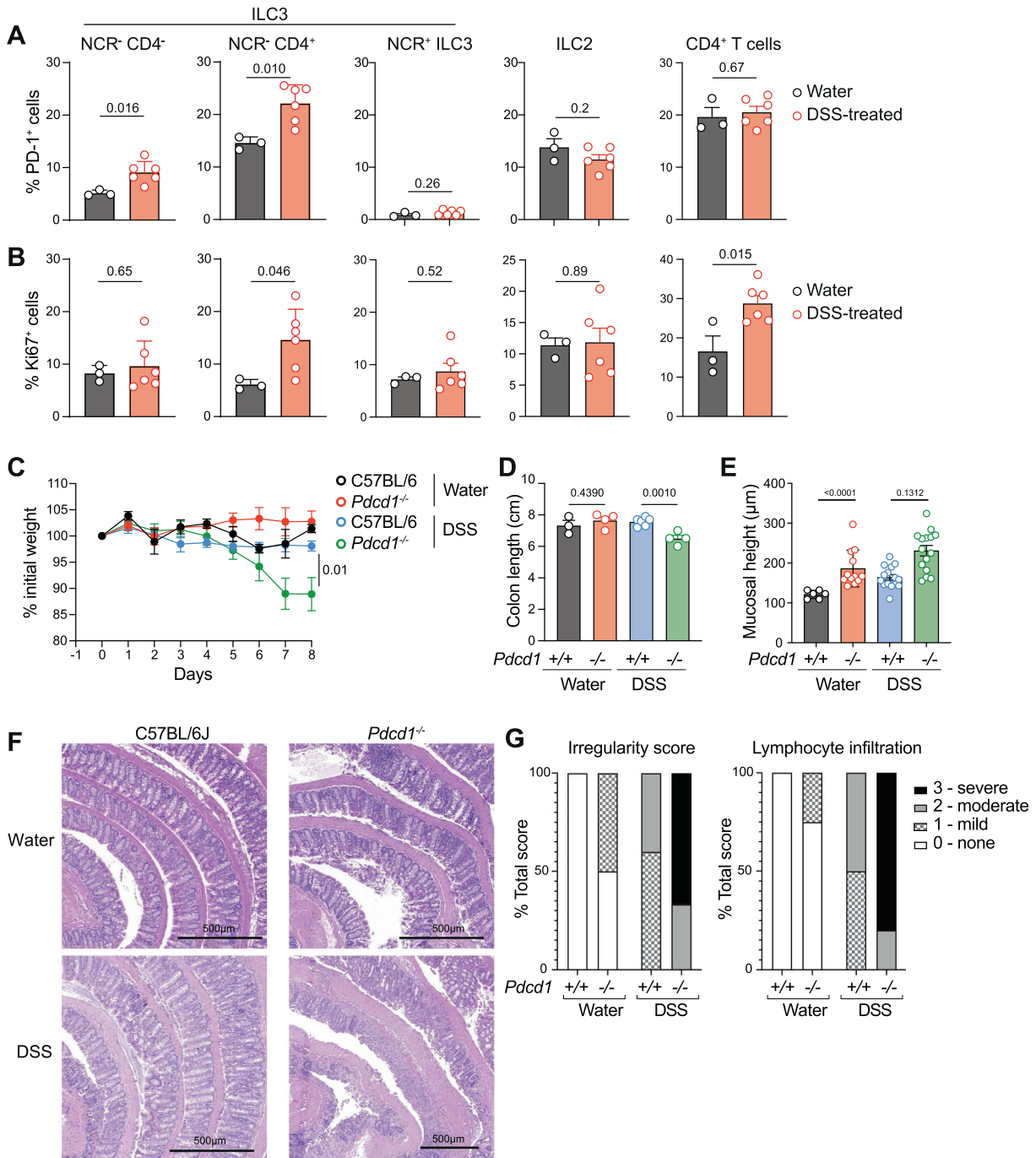


**Fig. 6** DSS treatment induces PD-1 on CD4<sup>+</sup> NCR<sup>-</sup> ILC3 that are required to control intestinal inflammation. (A, B) Frequencies of PD-1<sup>+</sup> (A) and Ki-67<sup>+</sup> (B) cells among the ILC3 subsets, ILC2 and CD4<sup>+</sup> T cells isolated from C57BL/6 mice treated or not with DSS for 3 days. Data show one representative experiment of two similar experiments ( $n = 3-6$  mice/genotype/experimental group). (C-G) PD-1-sufficient (C57BL/6) and deficient mice (*Pdcd1*<sup>-/-</sup>) were co-housed for 10 days and either given 2% DSS (wt/vol) in water or only water for 5 days followed by 3 days of untreated water then analyzed on day 8. (C) Weight is shown as a percentage of the initial weight. (D, E) Colon length (D) and quantitative analysis of crypt height (E) of C57BL/6 and *Pdcd1*<sup>-/-</sup> mice treated with DSS or kept underwater on day 8. (F) Hematoxylin and eosin-stained sections of the colon of C57BL/6 and *Pdcd1*<sup>-/-</sup> mice treated or not with DSS. (scale bar, 500 µm). (G) Epithelial irregularity and inflammatory infiltrate were scored from three sections over two different slides per mouse (0 = normal/none; 1 = minor; 2 = moderate; 3 = severe). Analyses were performed across six randomly selected sites per mouse. (A-E) Data show mean  $\pm$  SD. Statistical analyses were performed using unpaired Student's t tests. The p values are indicated. CD = cluster of differentiation; DSS = dextran sulfate sodium; ILC3 = intestinal group 3 innate lymphoid cells; NCR = natural cytotoxicity receptor; PD-1 = programmed cell death 1; SD = standard deviation.

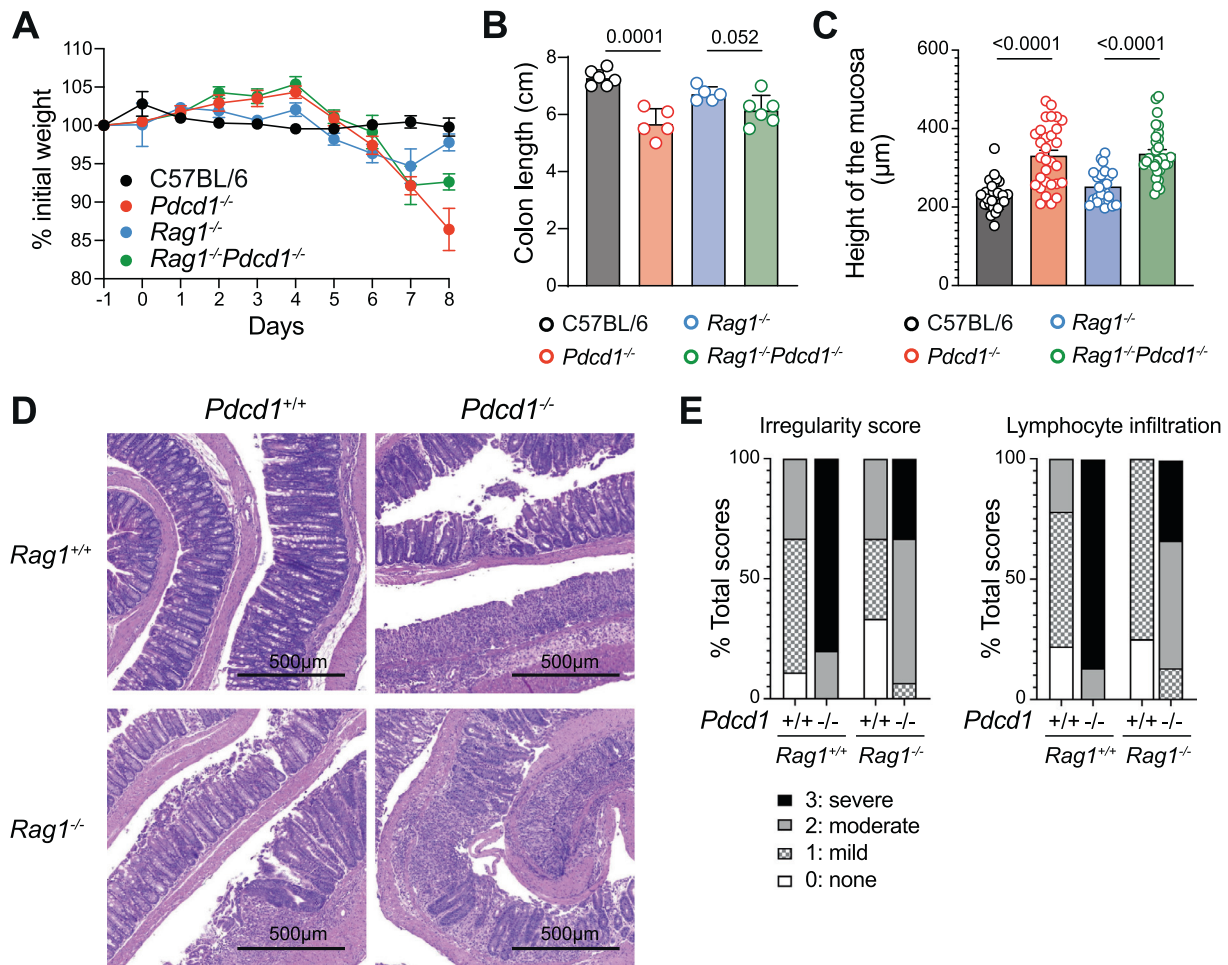


**Fig. 7** Loss of PD-1 expression increases the susceptibility of mice to inflammation following DSS treatment. (A–E) C57BL/6, *Pdc1*<sup>-/-</sup>, *Rag1*<sup>-/-</sup>, and *Rag1*<sup>-/-</sup>*Pdc1*<sup>-/-</sup> mice were either given 2% DSS (wt/vol) in water or only water for 5 days followed by 3 days of untreated water and then analyzed on day 8. (A) Weight is shown as a percentage of the initial weight. (B, C) Colon length (B) and height of the mucosa (C) on day 8 are shown. (D) Representative hematoxylin and eosin-stained sections of tissues. (scale bar, 500 µm). (E) Quantitative analysis of epithelial irregularity and inflammatory infiltrate scored from three sections over two different slides per mouse (0 = normal/none; 1 = minor; 2 = moderate; 3 = severe). Analyses were performed across six randomly selected sites per mouse. (A–E) Data show mean ± SD. Statistical analyses were performed using unpaired Student's t tests. The *p* values are indicated. DSS = dextran sulfate sodium; PD-1 = programmed cell death 1; SD = standard deviation.

assess their mitochondrial mass and membrane potential, respectively. We observed increased mitochondrial mass (MitoTracker Green; Fig. 5G) and reduced mitochondrial potential (MitoTracker Deep Red) (Supplementary Figs. 5A and 5B) associated with augmented mitochondrial depolarization in intestinal PD-1<sup>+</sup>NCR<sup>-</sup> ILC3 (Fig. 5H). Increased expression of uncoupling proteins, particularly *Trp53inp1* and *Slc25a14*, was previously found to be associated with the accumulation of reactive oxygen species in cells as a preservative mechanism to counteract the accumulation of reactive oxygen species (ROS) in the mitochondria produced during oxidative phosphorylation, maintaining the Red-ox balance to avoid mitochondrial oxidative stress<sup>39,40</sup>. Indeed, while we observed increased glucose and lipid uptakes and *Hk3* expression, suggesting the fueling of the tricarboxylic acid cycle and oxidative phosphorylation, we found no difference in the level of cellular ROS in PD-1<sup>+</sup>NCR<sup>-</sup> ILC3 compared to PD-1<sup>-</sup> cells (Supplementary Figs. 5C and

5D). However, the mitochondrial ROS were increased in PD1<sup>+</sup> ILC3 indicating an enhanced mitochondrial respiration metabolism in PD1<sup>+</sup> ILC3 (Fig. 5). Altogether, these results indicate a metabolic adaption of PD-1<sup>+</sup>NCR<sup>-</sup> ILC3 to sustain their activity while preserving their integrity from ROS-induced oxidative stress.

#### PD-1 expression promotes and sustains gut homeostasis

To elucidate the regulation of PD-1 after the disruption of homeostasis, mice were treated with DSS to induce intestinal epithelial damage. Following DSS treatment, PD-1 expression on ILC3 was increased compared to C57BL/6 control animals. Upon inflammation NCR<sup>+</sup> ILC3 did not significantly upregulate PD-1 while NCR<sup>-</sup> subsets, notably the CD4<sup>+</sup> ILC3 responded by a strong upregulation of PD-1 (Fig. 6A). The upregulation of PD-1 in NCR<sup>-</sup>CD4<sup>+</sup> ILC3 was associated with increased proliferation (Fig. 6B). Other lymphocytes such as T cells and ILC2 did not

upregulate PD-1 following treatment (Fig. 6A). These data indicate that the NCR<sup>+</sup>CD4<sup>+</sup> ILC3 subset is particularly sensitive to homeostatic changes and upregulates PD-1 in response to DSS-induced inflammation.

To determine whether PD-1 plays a role in the control of gut inflammation, we evaluated the response of *Pdcd1*<sup>-/-</sup> mice to DSS-induced colitis. We co-housed wild-type and *Pdcd1*<sup>-/-</sup> mice for 10 days and treated them with 2% DSS for 5 days and then returned to normal water for 3 days before analysis (Fig. 6). Wild-type mice did not lose a significant amount of weight and showed only limited inflammation and infiltration in the colon after DSS treatment compared with control mice maintained on water alone (Fig. 6C). However, *Pdcd1*<sup>-/-</sup> animals showed significant weight loss (Fig. 6C) and serious disruption of the intestinal barrier integrity characterized by an increase of the inflammatory infiltrate and epithelial damage (Figs. 6D and 6E). Interestingly, histological analyses of the colon collected from *Pdcd1*<sup>-/-</sup> mice at steady-state have revealed a small but consistent increase of lymphocyte infiltration and an alteration of the epithelial barrier observed by histology including the height or the irregularity of the mucosa (Figs. 6F and 6G). These results suggest that the constitutive expression of PD-1 acts to maintain intestinal homeostasis, dampening inflammatory responses in the gut.

To distinguish the contribution of PD-1 loss in the innate versus adaptive immune compartments observed in the DSS-treated *Pdcd1*<sup>-/-</sup> mice, we next compared the inflammatory response in *Rag1*<sup>-/-</sup> and *Rag1*<sup>-/-</sup>*Pdcd1*<sup>-/-</sup> mouse strains (Fig. 7). While *Rag1*<sup>-/-</sup> mice, which lack adaptive immune cells, were less susceptible to colitis compared to the *Rag1*<sup>+/+</sup> as previously shown<sup>41</sup>, the loss of PD-1 in *Rag1*<sup>-/-</sup> mice led to an increase in both weight loss and mucosal height in the large intestine of DSS-treated animals compared with *Rag1*<sup>-/-</sup> mice (Figs. 7A–C). This observation correlated with increased levels of inflammation and cell infiltration in the DSS-treated groups (Figs. 7D and 7E). Collectively, our data show that PD-1 is upregulated on NCR<sup>+</sup>CD4<sup>+</sup> ILC3 after disruption of the intestinal barrier, and its expression is required to control the inflammation and return to homeostasis.

## DISCUSSION

Immune checkpoints negatively regulate tumor immunity and responses to infections. The development of blocking antibodies targeting these immunological brakes reinstated potent anti-tumor responses, improving cancer patient outcomes. Despite being first identified as a key regulatory mechanism involved in the maintenance of tissue homeostasis, little is known about how these checkpoint molecules impact gut homeostasis and responses to inflammation. In this study, we show that PD-1 signaling is an important regulator of the IL-22 pathway in ILC3, known to promote barrier repair. Although a relatively small proportion of ILC3 expresses PD-1 at steady-state, PD-1 expression was enriched in a specific population of ILC3 cells, namely the VIPR2<sup>+</sup> CCR6<sup>+</sup> subset, which are strategically placed in the lamina propria, and has been established as critical for maintaining gut homeostasis<sup>15,16</sup>. Following intestinal inflammation, NCR<sup>+</sup> ILC3 specifically upregulated PD-1 while other lymphocytes that also constitutively express this receptor remained unchanged. The lack of PD-1 in the innate compartment was associated with an increased susceptibility to colitis and reduced capability to control inflammation.

We found that PD-1<sup>+</sup> ILC3 were mainly localized in the cryptopatches and were enriched in the CD4<sup>+</sup> subsets. PD-1<sup>+</sup> ILC3 were more abundant in newborn mice and slowly decreased with time until 3 weeks of age and remained stable in adulthood. This increased expression of PD-1 during the first weeks of life correlated with the proliferation of the ILC3 during this period. In the course of inflammation, we also observed a positive correlation between upregulation of PD-1 and proliferative capacity of the ILC3. Functionally, PD-1<sup>+</sup> ILC3 displayed enhanced activity compared with their PD-1<sup>-</sup> counterparts. In contrast to the role of PD-1 in ILC2 which has been shown to limit the production of IL-5, proliferation, and glycolysis<sup>27</sup>, we found that PD-1 in ILC3 promoted proliferation, metabolic activity, and cytokine production. Wu et al. recently showed that PD-1 was limiting fatty acid oxidation to sustain IL-22 production after activation<sup>26</sup>. Our data showed that PD-1<sup>+</sup> ILC3 displayed increased activity of other metabolic pathways known to sustain IL-22 production including the glycolysis and the polyamine synthesis<sup>37,38</sup>. Interestingly, PD-1<sup>+</sup> ILC3 also showed increased expression of antioxidants that prevented the accumulation of ROS in ILC3. *In vitro* analyses showed that PD-1 expression was inhibited by Notch signaling, potentially explaining the absence of PD-1 expression on NCR<sup>+</sup> ILC3 that requires Notch ligands to develop from NCR<sup>-</sup> ILC3. While IL-23 stimulation increased the expression of PD-1 at the surface of NCR<sup>+</sup> ILC3 even in presence of OP9-DL1, we could not observe an upregulation of PD-1 on NCR<sup>+</sup> ILC3 after DSS-induced inflammation.

Previous work highlighted the importance of PD-1 expression on intestinal immune cells, particularly Tfh cells, for Immunoglobulin A production and for controlling microbiota composition and tissue homeostasis<sup>42,43</sup>. We found that the microbiota was a key driver of PD-1 expression at homeostasis in adulthood. We observed that the highest expression of PD-1 in ILC3 residing in the colon where bacteria are most densely concentrated, ~10<sup>12</sup> bacteria/gram, compared with the small intestine that contains between 10<sup>3</sup> to 10<sup>7</sup> bacteria/gram intestinal content<sup>44</sup>. This is in keeping with previous studies that revealed gut microbiome dysbiosis with a severe reduction in the number of “healthy” bacteria such as *Bifidobacterium* and *Bacteroidaceae* and an increase in bacteria such as *Alcaligenaceae* associated with tissue pathology in mice lacking PD-1<sup>43</sup> or ILC<sup>3</sup>. Furthermore, we observed increased intestinal inflammation following DSS treatment in mice deficient for PD-1 expression compared with wild-type mice. We recapitulated this observation in *Rag1*<sup>-/-</sup> mice, lacking both T and B lymphocytes, indicating that PD-1 expression on ILCs is required, at least partially, to control inflammation following DSS treatment. Collectively, these observations highlight the significance of this PD-1/PD-L1 axis on intestinal immune cells in maintaining gut homeostasis and the two-way communication paths that exist between the mucosa and the microbiota.

It is also of interest that these gastrointestinal bacterial species are also beneficial for the efficacy of immune checkpoint inhibitor therapy<sup>45–47</sup>. For example, mice treated with broad-spectrum antibiotics or germ-free mice that lacked the intestinal commensals *Bifidobacterium* were resistant to anti-(PD-(L)1) Programmed death-ligand 1 therapies<sup>45,46,48</sup>. Furthermore, these intestinal species were found to be increased in cancer patients who responded to treatments, potentially through increased dendritic cell function and enhanced CD8<sup>+</sup> T cell priming in the tumor microenvironment<sup>46</sup>. However, the consequences of gut dysbiosis on intestinal immunity have remained elusive.

Here we found that disrupting gut colonization with intestinal commensals strongly reduced PD-1 expression on T cells, ILC2, and ILC3. These results suggest that the microbiota directly shape intestinal immunity and fine-tune immune checkpoint expression on immune cells to maintain gut homeostasis. By extending these observations to tumor-bearing mice or cancer patients, this would offer a rationale behind the role of intestinal microbiota in anti-tumor immunity and responses to immune checkpoint blockers, warranting further investigations.

The role of checkpoint molecules has been mainly explored in cytotoxic lymphocytes, our study highlights the multifaceted functions of PD-1 and how this immune checkpoint fine-tunes ILC-dependent immune protection. Preclinical observations suggest that targeting PD-1 on ILC2 could be beneficial in pancreas adenocarcinoma<sup>22</sup> and melanoma<sup>21</sup>, or the targeting of PD-1 on ILC3 found in mesothelioma and metastatic tumors<sup>49</sup>. Recently, a loss of ILC3 expressing the major histocompatibility complex class II (MHC-II) has been associated with resistance to anti-PD-1 treatment in response to MC38 colon tumor or melanoma<sup>50</sup>. Given that, in addition to MHC-II expression<sup>51</sup>, NCR<sup>-</sup> ILC3 constitutively expresses PD-1, it may be pertinent to take into account the impact of anti-PD-1 antibodies on ILC activity and intestinal inflammation. These findings could have a broader implication in our understanding of responsiveness to checkpoint inhibitors and could pave the way for modulating intestinal immunity together with the gut microbiota with the ultimate goal of further improving the efficacy of current cancer immunotherapy approaches.

## METHODS

### Mice

C57BL/6 (B6; strain 000664), *Pdcd1*<sup>-/-</sup> (*Pdcd1*<sup>tn1.15hr/J</sup>; strain 021157)<sup>52</sup>, *Rorc*(*yt*)<sup>+/-GFP53</sup> (strain 07572), *Rag1*<sup>-/-</sup> (*Rag1*<sup>tm1Mom</sup>) (strain 002216)<sup>54</sup>, *Rag1*<sup>-/-</sup> *Pdcd1*<sup>-/-52</sup>, *Csf2*<sup>BFP/YFP55</sup> mice were maintained on a C57BL/6 (Ly5.2<sup>+/+</sup>, CD45.2<sup>+/+</sup>) background and have been described previously. B6.SJL-*Ptprc*<sup>a</sup>*Pep3*<sup>b</sup>/BoyJ (Ly5.1<sup>+/+</sup>, CD45.1<sup>+/+</sup>; strain 002014) and CD45.1<sup>+</sup>CD45.2<sup>+</sup>(F1) mice were used for mixed BM chimeric experiments. Mice were bred and maintained in specific pathogen-free conditions at the Walter and Eliza Hall Institute of Medical Research and the University of Queensland Frazer Institute and germ-free C57BL/6 mice were bred and maintained at the University of Queensland Frazer Institute. Both male and female mice 6–16 weeks old were used. Animals were handled according to the guidelines of the Australian Code for the Care and Use of Animals of the National Health and Medical Research Council of Australia and experimental procedures were approved by the Institutional Animal Ethics Committee of the Walter and Eliza Hall Institute of Medical Research and the University of Queensland Frazer Institute.

### Isolation of lymphoid cells

The small intestine and caecum/large intestine were cleaned, Peyer's patches and caecal patches were removed, then the intestine was cut longitudinally before being minced into small pieces approximately 1–2 mm length. Single-cell suspensions of lymphocytes were isolated from the small intestine and caecum/large intestine following incubation for 40 minutes at 37°C in calcium ion and magnesium ion free Hanks media containing 2% (v/v) heat-inactivated fetal calf serum (FCS) and 5 mM (EDTA) Ethylenediaminetetraacetic acid with gentle shaking to remove intestinal epithelial cells<sup>35,56</sup>. The supernatant was discarded,

and tissues were then incubated, with gentle shaking, for 45 minutes with 1 mg/mL (w/v) Collagenase type IV (Worthington, USA), 200 µg/mL DNase I (Roche, Switzerland), 4 U/mL Dispase (Sigma, USA) in RPMI-1640 + 2% FCS at 37°C. Preparations were filtered and mononuclear cells were isolated by centrifugation on a 40%–80% Percoll gradient. Lymphocytes were recovered from the interface and washed in (FACS) Fluorescence-Activated Cell Sorting buffer. Single-cell suspensions were generated from mLN by gently dissociating tissues using 70 µm filters. Cells were resuspended in FACS buffer.

### Flow cytometry

Single-cell suspensions were stained with the following antibodies: TCRβ (H57-597), CD19 (6D5), CD3 (17A2), NK1.1 (PK136), TCRγδ (GL3), Ter119 (TER-119), Gr1 (RB6-8C5), and CD11b (M1/10), EPCAM (G8.8) (all from BioLegend, USA); CD19 (1D3), CD3ε (145-2C11), ICOS (C398.4A), NKp46 (29A1.4), NK1.1 (PK136), CD117 (2B8), CD127 (IL-7R, A7R34), Sca-1 (D7), B220 (RA3-6B2), CD11c (N418), CD4 (GK1.5), PD-L1 (M1H5) and KLRG1 (2F1) (all from eBioscience); CD45.1 (A20), CD45.2 (104), CD45 (30F11), CD90.2 (30-H12), CCR6 (140706), PD-1 (J43), CD103 (M290), CD11b FITC (M1/70) CD64 (X54-5/7.1) IA/IE (M5/114), Ly6G (1A8) and CD49a (Ha31/8) (all from BD Biosciences, USA); CD4 (GK1.5, in house) together with the fixable viability dye 700 (BD Horizon<sup>TM</sup>, USA) or eF506 (eBioscience). Intracellular staining was performed using the Transcription Factor Staining Buffer Set (eBioscience) and antibodies against GATA-3 (TWAJ, BD Biosciences), Roryt (AFKJS-9, BD Biosciences) and Eomesodermin (Dan11mag, eBioscience) and cytokines IL-17A (eBio17B7, eBioscience) and IL-22 (IL22JOP, eBioscience). Cells were analyzed using a Fortessa X20 (BD Biosciences) and FlowJo software (USA) version 10.5.3 was used for analysis. The cytokine expression of ILC3 was determined using the following conditions: single-cell suspensions were stimulated for 4 hours in complete RPMI-1640 containing 10% heat-inactivated FCS, 1 mM L-glutamine, 100 U/mL penicillin, 100 µg/mL streptomycin and 50 µM β-mercaptoethanol in the presence of 10 ng/mL recombinant (r)IL-7, 10 ng/mL (rIL) recombinant interleukin-23 (R&D Systems, USA), and GolgiStop<sup>TM</sup> (BD Biosciences). To test the constitutive secretion of cytokines, cells were incubated 4h in the presence of 10 ng/mL rIL-7 and GolgiStop<sup>TM</sup>.

### Metabolic staining

Cell suspensions or purified ILC3 from the small intestine were incubated in glucose-free (RPMI) Roswell Park Memorial Institute in the presence of 2-NBDG (30 µM, Invitrogen) for 20 minutes. For lipid uptake and neutral lipid staining, ILC3 was stained with Bodipy 493/503 or Bodipy<sup>TM</sup>FLC<sub>16</sub> (200 µM, Invitrogen) in serum-free media for 30 minutes at 37°C. For Polyamine staining, cells were incubated with PolyamineRED (30 µM, Funakoshi, Japan) in serum-free media for 15 minutes at 37°C. After two washes in cold FACS buffer, cells were stained with the surface antibodies for 30 minutes on ice, washed, and analyzed immediately using a Fortessa X20 (BD Biosciences, USA). To detect mitochondrial ROS, cells were incubated with MitoSOX Red (5 µM, Invitrogen, USA) for 30 minutes at 37°C. To detect mitochondrial mass and potential, cells were stained with MitoTracker Green FM (100 nM, Invitrogen) and MitoTracker Deep Red FM (10 nM, Invitrogen) for 30 minutes at 37°C.

### Histology and confocal imaging

For histological analyses, tissues were fixed in 10% neutral buffered formalin and processed for wax embedding and routine hematoxylin and eosin staining. Tissues were analyzed with an Aperio ImageScope v11.2.0.780 software (Leica, Germany) and features were scored for the presence of mucosal ulceration, mucosal height, epithelial irregularity, and lymphocyte infiltration using the grading system: 0 = no changes, 1 = mild changes, 2 = moderate changes and 3 = severe changes.

For confocal imaging analysis, intestinal tissues from *Rorc*( $\gamma$ )<sup>t+/GFP</sup> mice were gently flushed with phosphate buffered saline (PBS) phosphate buffered saline, fixed in 4% paraformaldehyde for 4 hours at 4°C and cryoprotected by overnight infiltration with 30% sucrose at 4°C. Tissues were then cut longitudinally and curled into a “Swiss roll” for visualization of the full length of the tissue. The “Swiss roll” was embedded in OCT (Optimal cutting temperature compound) and frozen at -80°C. 10  $\mu$ m thick cryosections were cut onto Superfrost Plus (Fisherbrand, USA) slides and air dried. Slides were washed once with PBS and blocked with PBS containing 1% BSA (Bovine serum albumin), 3% normal goat serum, 0.01% Triton X-100 for 30 minutes at room temperature. Tissue sections were then rinsed in staining buffer (0.1% BSA, 0.3% normal goat serum 0.01% Triton X-100 in PBS) and incubated with anti-GFP Alexa 488 (1/400, Invitrogen), anti-PD-1 PE/Dazzle 594 (1/50, RMP1-30, BioLegend), anti-CD3 $\epsilon$  eFluor 450 (1/200, 17A2, Invitrogen), anti-EpCAM (CD326) Alexa 647 (1/500, G8.8, BioLegend) and anti-NKp46 biotin (1/100, AF2225, R&D). Tissue sections were stained overnight at 4°C with antibodies diluted in the staining buffer. Sections were then washed three times and mounted with ProLong Diamond mounting medium with or without (DAPI) 4',6-diamidino-2-phenylindole (Invitrogen). Images were acquired on a Zeiss (Germany) LSM880 NLO confocal microscope.

### Oral antibiotic treatment

Mice were given unrestricted access to drinking water containing a mix of ampicillin (1 mg/mL), streptomycin (5 mg/mL) and colistin (1 mg/mL) (Sigma) for 3 weeks<sup>47,57,58</sup>. Antibiotics efficacy was macroscopically observed through the enlargement of the caecum compared with antibiotics-free mice.

### Chimeric mice

Mixed BM chimeric mice were generated by reconstituting lethally irradiated (2  $\times$  5.5 Gy) Ly5.1 (CD45.1<sup>+</sup>) recipient mice with a 1:1 mixture of *Pdcd1*<sup>-/-</sup> (CD45.2<sup>+</sup>) and C57BL/6  $\times$  Ly5.1 (CD45.2<sup>-</sup>CD45.1<sup>+</sup>) BM. A total of 5  $\times$  10<sup>6</sup> BM cells were injected/recipient. After 7–8 weeks reconstitution, mice were analyzed.

### Dextran sodium sulfate treatment

Dextran sodium sulfate (molecular mass 36,000–50,000 Da; MP Biomedicals, USA) was added into drinking water 2% (w/v) for 5 days followed by 3 days of regular water. Weight loss, stool consistency, and hematochezia were monitored daily, and mice were analyzed on day 8 after commencing treatment.

### ILC3 isolation and *in vitro* culture with OP9 stromal cells

Cells isolated by digestion from the small intestinal tissue were stained for 30 minutes with optimally-titrated antibodies against CD90.2, NKp46, NK1.1, CD117, IL-7R $\alpha$ , PD-1, KLRG1, B220, CD19, CD3, CD11b and CD45. ILC3 were identified as live CD45<sup>+</sup>CD90.2<sup>+</sup>CD117<sup>+</sup>IL-7R $\alpha$ <sup>+</sup> and negative for KLRG1, NKp46, PD-1, B220, CD19, CD3 $\epsilon$ , CD11b and NK1.1. Stained cells were washed

and sorted using FACS ARIA III (BD Biosciences). Purified NCR<sup>-</sup>PD-1<sup>-</sup> ILC3 were cultured in complete media in the presence of rIL-7 (10 ng/mL), SCF (Stem cell factor, 10 ng/mL), Flt3L (Fms-like tyrosine kinase 3 ligand, 10 ng/mL) or with rIL-7 (10 ng/mL) and rIL-23 (10 ng/mL) for 8 days before analysis of NKp46 and PD-1 expression.

### Single-cell RNA sequencing and data analysis

Live/Dead<sup>-</sup>CD45<sup>+</sup> Lin<sup>-</sup> (CD3, CD11b, B220, TER119, TCR $\beta$ , CD19, NK1.1, F4/80) CD127<sup>+</sup> immune cells were sorted from small intestines of C57BL/6 mice ( $n$  = 3). Cells were incubated with 0.1  $\mu$ g TotalSeq-A HashTags (BioLegend) prior to FACS according to manufacturer's instructions to label samples. The sorted cells were then incubated with TotalSeq-A antibodies (BioLegend) a second TotalSeq-A HashTag 0.1  $\mu$ g to label sub-populations. cells were loaded per 10X 3'-HT capture and a total of two capture reactions were performed on the Chromium X platform (10X Genomics, USA). scRNAseq libraries and HashTag and antibody libraries were generated according to manufacturer's instructions. Libraries were sequenced on an Illumina NextSeq 2000 platform. Reads were processed by 10X Cell Ranger v.7 using the mm10 reference genome. scRNAseq data were further processed and analyzed using R v.4.2.0 and the Seurat package v. 4.0.6113. Demultiplex step was performed with DemuxMix v0.9.9.6 to determine the identity of each sample based on HashTag number<sup>59</sup>. Cells with fewer than 200 genes detected, more than 50,000 genes detected, or more than 10% mitochondrial reads were then removed. Data were normalized using NormalizeData function. The 3000 most variable genes for each sample were identified using FindVariableFeatures using “vst” selection method. The expression of all genes was then scaled using ScaleData function. Principal component analysis on the feature genes selected above was performed with RunPCA algorithm. According to ElbowPlot results, 10 principal components were selected for the clustering of samples using FindNeighbors. FindClusters with resolution 0.4 was then run to identify different clusters. FindAllMarkers was used to identify marker genes for each cluster using the Wilcoxon test on the raw counts. Cluster was determined by manual annotation based on knowledge. RunUMAP was used to perform dimensionality reduction by Uniform manifold approximation and projection (UMAP) using 10 largest principal components. Differential expressed gene analysis was run using FindAllMarkers using Wilcoxon rank sum test and Bonferroni correction. All plots of scRNAseq data were generated using the Seurat package as well as ggplot2 v.3.3.6. The Gene Expression Omnibus accession code for the sequencing data in this paper is GSE255270.

### Bulk RNA sequencing and analysis

CD45<sup>+</sup>Lineage<sup>-</sup> (CD3, CD11b, B220, TER119, TCR $\beta$ , CD19, NK1.1, F4/80) CD90.2<sup>+</sup>ROR $\gamma$ t<sup>+</sup> NCR<sup>-</sup>PD-1<sup>+</sup> and NCR<sup>-</sup>PD-1<sup>-</sup> ILC3 were purified by flow cytometric sorting (FACS Aria III; BD Biosciences) from the small intestine of female *Rorc*( $\gamma$ )<sup>t+/GFP</sup> mice. FACS-sorted ILC3 were washed twice in sterile PBS before being snap frozen and stored at -80 degrees until RNA extraction. Two biological replicates were generated for each subset from the small intestine from a pool of six mice. RNA was isolated using a QIAGEN (Netherlands) RNeasy Micro kit. Libraries were generated using the Clontech SMART-Seq v4 Ultra Low Input RNA Kit preparation (Takara, Japan), following the manufacturer's instructions. The libraries were then sequenced on Illumina NextSeq instrument

(Illumina, USA) using 2×76 base pair reads and 2×8 base pair indices.

Count data were pre-filtered. Genes were kept for analyses if their counts per million were larger than 0.5 in at least one group of samples, and genes related to immunoglobulins (Igh, Igkv) were filtered out. Differential gene expression was performed in R studio with Bioconductor package DESeq2 (version 1.34.0)<sup>60</sup>. Regularized log transformation (base 2)<sup>60</sup> was conducted in significantly differentially expressed genes (log2 fold change > 1 and adjusted  $p < 0.1$ ) for heatmap visualization. Pathway-enrichment analysis with Kyoto Encyclopedia of Genes and Genomes database was also performed on these significantly differentially expressed genes with Bioconductor package clusterProfiler (version 4.2.1)<sup>61,62</sup>. Heatmap of differentially expressed genes and bar plot of pathway-enrichment results were generated by R package pheatmap (version 1.0.12) and Bioconductor enrichplot (version 1.14.1), respectively. The Gene Expression Omnibus accession code for the sequencing data in this paper is GSE254794.

### Statistical analyses

All statistical analyses were performed with GraphPad Prism software (version 7.0 or 8.0, GraphPad Software, USA) with the exception of the RNA sequencing data. For more than two groups, statistical analyses were performed using analysis of variance followed by Tukey's multiple-comparison test or pairwise comparisons with Bonferroni adjustments. Otherwise, for two groups, statistical analyses were performed using the paired or unpaired Student's  $t$  tests. Results are shown as the mean  $\pm$  SD. Correlations between two variables were assessed using non-parametric Spearman correlation tests. Pooled data from at least two independent experiments are preferentially depicted. Otherwise, a representative experiment is shown out of, at least, two experiments performed yielding similar results. The  $p$  values were two-sided with 95% confidence intervals and considered significant at  $p < 0.05$ .

### AUTHOR CONTRIBUTIONS

Conceptualization: N.J., G.T.B and C.S. Investigation, validation, and analyses: N.J., L.X., C.S., Q.H., W.H.J.C., Q.H., H.Y. Processing scRNAseq: A.S., C.J.A.A, T.H.B, P.F.H, D.A.Z. Supervision: P.O., N. J., S.L.N, G.T.B, and C.S; Funding acquisition: N.J., G.T.B., C.S.; Manuscript: Original draft N.J., G.T.B., C.S.; Writing – Review & Editing, N.J., C.S., G.T.B with the input of all the coauthors. All authors reviewed, edited, provided input, and approved the manuscript before submission.

### DECLARATIONS OF COMPETING INTEREST

The authors declare they have no competing interests.

### FUNDING

This work was supported by grants and fellowships from the National Health and Medical Research Council (NHMRC) of Australia (1165443, 1122277, 1054925, 1135898 and 2008542 to G.T.B., 1165443, 1123000 and 2008090 to C.S.), a grant to The University of Queensland Chair of Immunology (Frazer Institute, G.T.B.), MS Australia (19-0614), Cancer Council NSW (RG 21-05 to G.T.B. and N.J.), Cure Cancer Australia and Cancer Australia through the Cancer Australia Priority-driven Cancer Research Scheme (1163990 N.J.), Alberta Cancer Foundation/Arnie Charbonneau Cancer Institute laboratory start up package (N.J.),

Canadian Cancer Society Emerging Scholar Research Grant (grant #708072, to NJ), the Dr. Robert C. Westbury Fund for Melanoma Research (N.J.), scholarships of the Australian Government Research Training Program (Q.H.), Melbourne Research Scholarship (W.C) and University of Queensland International Student Scholarship (H.Y) a CIHR Foundation Grant (P.S.O.). The Translational Research Institute is supported by a grant from the Australian Government; WEHI is supported through Victorian State Government Operational Infrastructure Support and Australian Government NHMRC Independent Research Institutes Infrastructure Support Scheme (IRISS).

### ACKNOWLEDGMENTS

We thank M. Camilleri, J. Janssen, S. Cree, S. Shaw, E. Mettes, J. Leahy, M. Chopin, J. Schreuder, and members of the Flow Cytometry, Histology, and BioServices facilities of the Walter and Eliza Hall Institute of Medical Research and Frazer Institute, University of Queensland for technical assistance and for helpful discussions. We thank M. Kates for technical advice on the use of fluorescent dyes for the metabolic profiling of ILC3.

### APPENDIX A. SUPPLEMENTARY DATA

Supplementary data to this article can be found online at <https://doi.org/10.1016/j.mucimm.2024.03.002>.

### REFERENCES

1. Sawa, S. et al. RORyt+ innate lymphoid cells regulate intestinal homeostasis by integrating negative signals from the symbiotic microbiota. *Nat. Immunol.* **12**, 320–326 (2011).
2. Guo, X. et al. Induction of innate lymphoid cell-derived interleukin-22 by the transcription factor STAT3 mediates protection against intestinal infection. *Immunity* **40**, 25–39 (2014).
3. Sonnenberg, G. F. et al. Innate lymphoid cells promote anatomical containment of lymphoid-resident commensal bacteria. *Science* **336**, 1321–1325 (2012).
4. Mao, K. et al. Innate and adaptive lymphocytes sequentially shape the gut microbiota and lipid metabolism. *Nature* **554**, 255–259 (2018).
5. Satoh-Takayama, N. et al. Microbial flora drives interleukin 22 production in intestinal NKp46+ cells that provide innate mucosal immune defense. *Immunity* **29**, 958–970 (2008).
6. Zenewicz, L. A. et al. Innate and adaptive interleukin-22 protects mice from inflammatory bowel disease. *Immunity* **29**, 947–957 (2008).
7. Zheng, Y. et al. Interleukin-22 mediates early host defense against attaching and effacing bacterial pathogens. *Nat. Med.* **14**, 282–289 (2008).
8. Huber, S. et al. IL-22BP is regulated by the inflammasome and modulates tumorigenesis in the intestine. *Nature* **491**, 259–263 (2012).
9. Hanash, A. M. et al. Interleukin-22 protects intestinal stem cells from immune-mediated tissue damage and regulates sensitivity to graft versus host disease. *Immunity* **37**, 339–350 (2012).
10. Ibiza, S. et al. Glial-cell-derived neuroregulators control type 3 innate lymphoid cells and gut defence. *Nature* **535**, 440–443 (2016).
11. Takatori, H. et al. Lymphoid tissue inducer-like cells are an innate source of IL-17 and IL-22. *J. Exp. Med.* **206**, 35–41 (2009).
12. Macho-Fernandez, E. et al. Lymphotoxin beta receptor signaling limits mucosal damage through driving IL-23 production by epithelial cells. *Mucosal Immunol.* **8**, 403–413 (2015).
13. Chen, V. L., Surana, N. K., Duan, J. & Kasper, D. L. Role of murine intestinal interleukin-1 receptor 1-expressing lymphoid tissue inducer-like cells in *Salmonella* infection. *PLoS One* **8**, e65405 (2013).
14. Lee, J. S. et al. AHR drives the development of gut ILC22 cells and postnatal lymphoid tissues via pathways dependent on and independent of Notch. *Nat. Immunol.* **13**, 144–151 (2011).
15. Seillet, C. et al. The neuropeptide VIP confers anticipatory mucosal immunity by regulating ILC3 activity. *Nat. Immunol.* **21**, 168–177 (2020).
16. Talbot, J. et al. Feeding-dependent VIP neuron-ILC3 circuit regulates the intestinal barrier. *Nature* **579**, 575–580 (2020).
17. Freeman, G. J. et al. Engagement of the PD-1 immunoinhibitory receptor by a novel B7 family member leads to negative regulation of lymphocyte activation. *J. Exp. Med.* **192**, 1027–1034 (2000).

18. Latchman, Y. et al. PD-L2 is a second ligand for PD-1 and inhibits T cell activation. *Nat. Immunol.* **2**, 261–268 (2001).
19. Taylor, S. et al. PD-1 regulates KLRG1+ group 2 innate lymphoid cells. *J. Exp. Med.* **214**, 1663–1678 (2017).
20. Yao, S. et al. PD-1 on dendritic cells impedes innate immunity against bacterial infection. *Blood* **113**, 5811–5818 (2009).
21. Jacquelot, N. et al. Blockade of the co-inhibitory molecule PD-1 unleashes ILC2-dependent antitumor immunity in melanoma. *Nat. Immunol.* **22**, 851–864 (2021).
22. Moral, J. A. et al. ILC2s amplify PD-1 blockade by activating tissue-specific cancer immunity. *Nature* **579**, 130–135 (2020).
23. Seillet, C. et al. Deciphering the Innate Lymphoid Cell Transcriptional Program. *Cell Rep.* **17**, 436–447 (2016).
24. Yu, Y. et al. Single-cell RNA-seq identifies a PD-1<sup>hi</sup> ILC progenitor and defines its development pathway. *Nature* **539**, 102–106 (2016).
25. Vacca, P. et al. PD-1 is expressed by and regulates human group 3 innate lymphoid cells in human decidua. *Mucosal Immunol.* **12**, 624–631 (2019).
26. Wu, D. et al. PD-1 signaling facilitates activation of lymphoid tissue inducer cells by restraining fatty acid oxidation. *Nat. Metab.* **4**, 867–882 (2022).
27. Helou, D. G. et al. PD-1 pathway regulates ILC2 metabolism and PD-1 agonist treatment ameliorates airway hyperreactivity. *Nat. Commun.* **11**, 3998 (2020).
28. Godinho-Silva, C. et al. Light-entrained and brain-tuned circadian circuits regulate ILC3s and gut homeostasis. *Nature* **574**, 254–258 (2019).
29. Mortha, A. et al. Microbiota-dependent crosstalk between macrophages and ILC3 promotes intestinal homeostasis. *Science* **343**, 1249288 (2014).
30. Elyahu, Y. et al. Aging promotes reorganization of the CD4 T cell landscape toward extreme regulatory and effector phenotypes. *Sci. Adv.* **5**, eaaw8330 (2019).
31. Mogilenko, D. A. et al. Comprehensive profiling of an aging immune system reveals clonal GZMK+ CD8+ T cells as conserved hallmark of inflammaging. *Immunity* **54**, 99–115.e12 (2021).
32. Sanos, S. L. et al. ROR $\gamma$ t and commensal microflora are required for the differentiation of mucosal interleukin 22-producing NKp46+ cells. *Nat. Immunol.* **10**, 83–91 (2009).
33. Mowat, A. M. & Agace, W. W. Regional specialization within the intestinal immune system. *Nat. Rev. Immunol.* **14**, 667–685 (2014).
34. Kinnebrew, M. A. et al. Interleukin 23 production by intestinal CD103+CD11b+ dendritic cells in response to bacterial flagellin enhances mucosal innate immune defense. *Immunity* **36**, 276–287 (2012).
35. Rankin, L. C. et al. The transcription factor T-bet is essential for the development of NKp46+ innate lymphocytes via the Notch pathway. *Nat. Immunol.* **14**, 389–395 (2013).
36. Chea, S. et al. Single-cell gene expression analyses reveal heterogeneous responsiveness of fetal innate lymphoid progenitors to Notch signaling. *Cell Rep.* **14**, 1500–1516 (2016).
37. Di Luccia, B., Gilfillan, S., Cella, M., Colonna, M. & Huang, S. C. C. ILC3s integrate glycolysis and mitochondrial production of reactive oxygen species to fulfill activation demands. *J. Exp. Med.* **216**, 2231–2241 (2019).
38. Peng, V. et al. Ornithine decarboxylase supports ILC3 responses in infectious and autoimmune colitis through positive regulation of IL-22 transcription. *Proc. Natl Acad. Sci. U. S. A.* **119**:e2214900119.
39. Seillier, M. et al. Defects in mitophagy promote redox-driven metabolic syndrome in the absence of TP53INP1. *EMBO Mol. Med.* **7**, 802–818 (2015).
40. Kwok, K. H. et al. Mitochondrial UCP5 is neuroprotective by preserving mitochondrial membrane potential, ATP levels, and reducing oxidative stress in MPP+ and dopamine toxicity. *Free Radic. Biol. Med.* **49**, 1023–1035 (2010).
41. Shalpour, S. et al. Interleukin-7 links T lymphocyte and intestinal epithelial cell homeostasis. *PLoS One* **7**, e31939 (2012).
42. Kawamoto, S. et al. The inhibitory receptor PD-1 regulates IgA selection and bacterial composition in the gut. *Science* **336**, 485–489 (2012).
43. Maruya, M., Kawamoto, S., Kato, L. M. & Fagarasan, S. Impaired selection of IgA and intestinal dysbiosis associated with PD-1-deficiency. *Gut Microbes.* **4**, 165–171 (2013).
44. Sekirov, I., Russell, S. L., Antunes, L. C. & Finlay, B. B. Gut microbiota in health and disease. *Physiol. Rev.* **90**, 859–904 (2010).
45. Matson, V. et al. The commensal microbiome is associated with anti-PD-1 efficacy in metastatic melanoma patients. *Science* **359**, 104–108 (2018).
46. Sivan, A. et al. Commensal *Bifidobacterium* promotes antitumor immunity and facilitates anti-PD-L1 efficacy. *Science* **350**, 1084–1089 (2015).
47. Vétizou, M. et al. Anticancer immunotherapy by CTLA-4 blockade relies on the gut microbiota. *Science* **350**, 1079–1084 (2015).
48. Zheng, Y. et al. Gut microbiome affects the response to anti-PD-1 immunotherapy in patients with hepatocellular carcinoma. *J. Immunother. Cancer* **7**, 193 (2019).
49. Tumino, N. et al. Presence of innate lymphoid cells in pleural effusions of primary and metastatic tumors: functional analysis and expression of PD-1 receptor. *Int. J. Cancer* **145**, 1660–1668 (2019).
50. Goc, J. et al. Dysregulation of ILC3s unleashes progression and immunotherapy resistance in colon cancer. *Cell* **184**, 5015–5030.e16 (2021).
51. Hepworth, M. R. et al. Innate lymphoid cells regulate CD4+ T-cell responses to intestinal commensal bacteria. *Nature* **498**, 113–117 (2013).
52. Keir, M. E., Freeman, G. J. & Sharpe, A. H. PD-1 regulates self-reactive CD8+ T cell responses to antigen in lymph nodes and tissues. *J. Immunol.* **179**, 5064–5070 (2007).
53. Eberl, G. et al. An essential function for the nuclear receptor ROR $\gamma$ (t) in the generation of fetal lymphoid tissue inducer cells. *Nat. Immunol.* **5**, 64–73 (2004).
54. Mombaerts, P. et al. RAG-1-deficient mice have no mature B and T lymphocytes. *Cell* **68**, 869–877 (1992).
55. Louis, C. et al. NK cell-derived GM-CSF potentiates inflammatory arthritis and is negatively regulated by CIS. *J. Exp. Med.* **217**, e20191421 (2020).
56. Rankin, L. C. et al. Complementarity and redundancy of IL-22-producing innate lymphoid cells. *Nat. Immunol.* **17**, 179–186 (2016).
57. Routy, B. et al. Gut microbiome influences efficacy of PD-1-based immunotherapy against epithelial tumors. *Science* **359**, 91–97 (2018).
58. Mielke, L. A. et al. TCF-1 limits the formation of Tc17 cells via repression of the MAF-ROR $\gamma$ t axis. *J. Exp. Med.* **216**, 1682–1699 (2019).
59. Klein, H. U. demuxmix: demultiplexing oligonucleotide-barcoded single-cell RNA sequencing data with regression mixture models. *Bioinformatics* **39**, btad481 (2023).
60. Love, M. I., Huber, W. & Anders, S. Moderated estimation of fold change and dispersion for RNA-seq data with DESeq2. *Genome Biol.* **15**, 550 (2014).
61. Yu, G., Wang, L. G., Han, Y. & He, Q. Y. clusterProfiler: an R package for comparing biological themes among gene clusters. *Omic* **16**, 284–287 (2012).
62. Wu, T. et al. clusterProfiler 4.0: A universal enrichment tool for interpreting omics data. *Innovation (Camb.)* **2**:100141.